metals

MDPI

Review

Mechanical Properties of Ti6Al4V Fabricated by Laser Powder Bed Fusion: A Review Focused on the Processing and Microstructural Parameters Influence on the Final Properties

Flávio Bartolomeu [1,2,*], Michael Gasik [3], Filipe Samuel Silva [1,2] and Georgina Miranda [4]

[1] CMEMS—UMinho, University of Minho, 4800-058 Guimarães, Portugal; fsamuel@dem.uminho.pt
[2] LABBELS—Associate Laboratory, 4800-058 Guimarães, Portugal
[3] Department of Materials Science and Engineering, School of Chemical Technology, Aalto University Foundation, Aalto, 00076 Espoo, Finland; michael.gasik@aalto.fi
[4] CICECO, Aveiro Institute of Materials, Department of Materials and Ceramic Engineering, University of Aveiro, 3810-193 Aveiro, Portugal; gmiranda@ua.pt
* Correspondence: flaviojorgebartolomeu@gmail.com

Abstract: Ti6Al4V alloy is an ideal lightweight structural metal for a huge variety of engineering applications due to its distinguishing combination of high specific mechanical properties, excellent corrosion resistance and biocompatibility. In this review, the mechanical properties of selective laser-melted Ti6Al4V parts are addressed in detail, as well as the main processing and microstructural parameters that influence the final properties. Fundamental knowledge is provided by linking the microstructural features and the final mechanical properties of Ti6Al4V parts, including tensile strength, tensile strain, fatigue resistance, hardness and wear performance. A comparison between Laser Powder Bed Fusion and conventional processing routes is also addressed. The presence of defects in as-built Ti6Al4V parts and their influences on the mechanical performance are also critically discussed. The results available in the literature show that typical Laser Powder Bed–Fused Ti6Al4V tensile properties (>900 MPa yield strength and >1000 MPa tensile strength) are adequate when considering the minimum values of the standards for implants and for aerospace applications (e.g., ASTM F136–13; ASTM F1108–14; AMS4930; AMS6932).

Keywords: additive manufacturing; laser powder bed fusion; microstructure; tensile strength; fatigue

Citation: Bartolomeu, F.; Gasik, M.; Silva, F.S.; Miranda, G. Mechanical Properties of Ti6Al4V Fabricated by Laser Powder Bed Fusion: A Review Focused on the Processing and Microstructural Parameters Influence on the Final Properties. *Metals* **2022**, *12*, 986. https://doi.org/10.3390/met12060986

Academic Editor: Antonio Mateo

Received: 5 May 2022
Accepted: 31 May 2022
Published: 8 June 2022

1. Introduction

In recent years, Additive Manufacturing (AM) has faced a tremendous process of maturation due to the great development of AM techniques and materials. AM has become one of the important topics of research, and from the industrial point of view, AM has been attracting the attention of manufacturing industries worldwide. The event "3D printing to the factory floor" is real, and it is occurring very quickly. Lux Research, Boston, Massachusetts, USA, a provider of tech-enabled research and innovation advisory services, has released a new report, "Will 3D Printing Replace Conventional Manufacturing?" which anticipates that the Additive Manufacturing market will reach USD 51 billion within a decade [1]. AM fabrication processes offer significant benefits for widespread industries, positively influencing society, the economy and the environment, increasing production sustainability. Some key benefits are pointed out in the following.

By using AM techniques, a physical part is directly and easily obtained from CAD data [2–4].

When using AM fabrication methods, tremendous product customization is possible without the extra costs usually associated with extra tools, dies, molds and others, which are higher in conventional processing routes such as casting or machining [5–7].

AM is triggering a revolutionary strategy in terms of engineering design, and AM techniques give clients, producers and users the possibility of designing with an exclusive

focus on the component function rather than manufacturing process difficulties [8,9]. Components with complex internal features would be almost impossible or unsustainable to produce using conventional manufacturing techniques [10–14]. AM opens new prospects to develop/fabricate a mechanical part regardless of its geometrical complexity [8,9].

AM's high design freedom and flexibility enable the production of lightweight components able to retain structural strength, despite exhibiting a significant reduction in weight. Several cellular or lattice structures have been proposed as advantageous solutions for new and disruptive biomedical solutions such as hip implants [15–19].

When using AM techniques, the material waste is almost zero, and no toxic chemicals are directly used, in contrast, for instance, to conventional machining [20,21].

AM has the capability of producing near-net-shape components with high geometrical and dimensional accuracy with the ability to combine several machining steps into a single production step, which dramatically reduces the fabrication time [6,13].

According to ISO 17296-2:2015 [22], AM techniques can be grouped into the following seven categories: VAT Photopolymerization, Material Jetting, Binder Jetting, Sheet Lamination, Material Extrusion, Directed Energy Deposition and Powder Bed Fusion. The present review is focused on the Laser Powder Bed Fusion (LPBF) technique, which is a Powder Bed Fusion technique. In LPBF, a laser beam is used as an energy source to melt powder beds [2,3]. CAD data are incorporated into the software of the equipment and then sliced into many layers. After ensuring an adequate operating atmosphere (typically argon), the first layer of powder is deposited over the build platform. Afterwards, the laser scans the pattern instructions for the respective layer, promoting the melting and fusion of powder. Subsequently, a new layer of powder is deposited over the previous one, melting the new powder and also promoting fusion to the previous layer. In this context, the huge potential of Laser Powder Bed Fusion has been used to design, develop and study new solutions for a wide range of applications. LPBF's high design freedom offers great potential for lightweight design and can bring to life completely new component designs by incorporating extraordinary tools, such as Topology Optimization, for achieving lightweight and high-performance components [23–25]. The production of Ti6Al4V components by Laser Powder Bed Fusion has been one of the important topics in research targeting custom-fitting solutions with high added value for aerospace, aeronautics and biomedical industries [26,27]. The present review aims to address the physicomechanical properties of LPBFed Ti6Al4V-based components in detail and analyze the main processing and microstructural parameters that influence the final properties.

2. Ti6Al4V Alloy

At room temperature, pure titanium displays a hexagonal close-packed (HCP) structure, named the α phase. At the β transus temperature (approximately 885 °C), this structure is transformed into a body-centered cubic (BCC) structure called the β phase [28,29]. Commonly, five classes are discerned: α alloys, near-α, α-β, near-β and β alloys. Ti6Al4V alloy is considered an α–β alloy that contains 6 wt % aluminum as the α stabilizer and 4 wt % vanadium as the β stabilizer [30,31]. For Ti6Al4V, the β transus temperature is approximately 995 °C under equilibrium conditions, so above this temperature, Ti6Al4V becomes 100% β phase [28,29]. The final microstructure is highly correlated to the cooling rate that occurs from above the β transus temperature [32]. Slow to intermediate cooling rates lead to the nucleation and growth processes of α-lamellae (α phase) to form α-Widmanstätten laths within the β matrix [33]. Such microstructures are commonly observed in wrought and cast components. As the cooling rate increases, the length and thickness of α-lamellae decrease, leading to enhanced mechanical strength [28]. Furthermore, when the cooling rate is sufficiently fast, the β phase undergoes a diffusionless transformation to the martensitic α' phase [32]. This transformation is an aspect of interest, because it increases the strength and hardness of this alloy, although reducing ductility. Figure 1 shows typical SEM images of cold rolling, hot rolling and Laser Powder Bed Fusion [3,34–36]. Figure 1c shows a finer microstructure of Ti6Al4V fabricated by LPBF. It exhibits the presence of the α' martensitic

phase with a needle-like feature as a consequence of the extremely high cooling rate [3,37]. Figure 2 shows typical TEM images of Ti6Al4V obtained by Electron Beam Melting (EBM) and Laser Powder Bed Fusion.

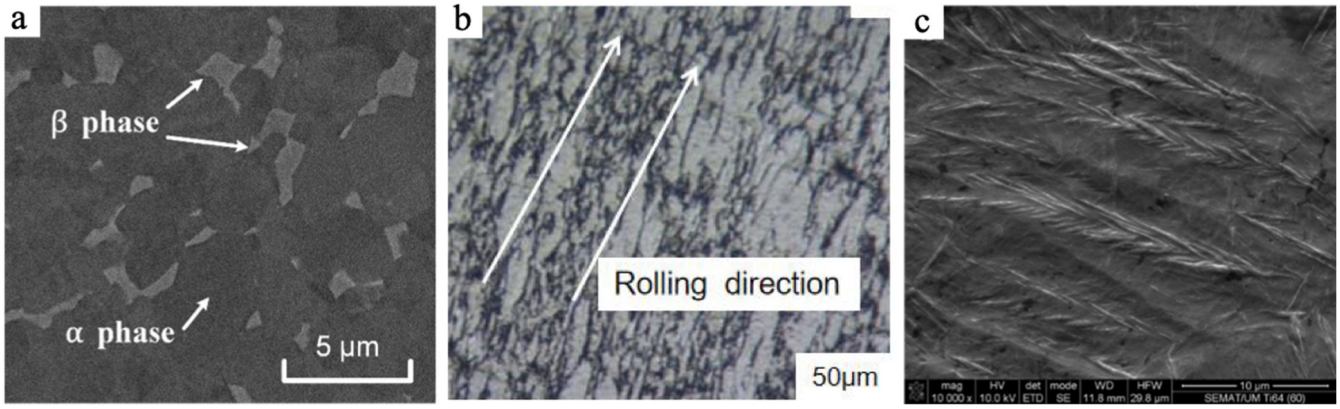

Figure 1. SEM images of Ti6Al4V obtained by (**a**) cold rolling, (**b**) hot rolling and (**c**) Laser Powder Bed Fusion (adapted with permission from [3,34,35]. Copyright 2016 Elsevier).

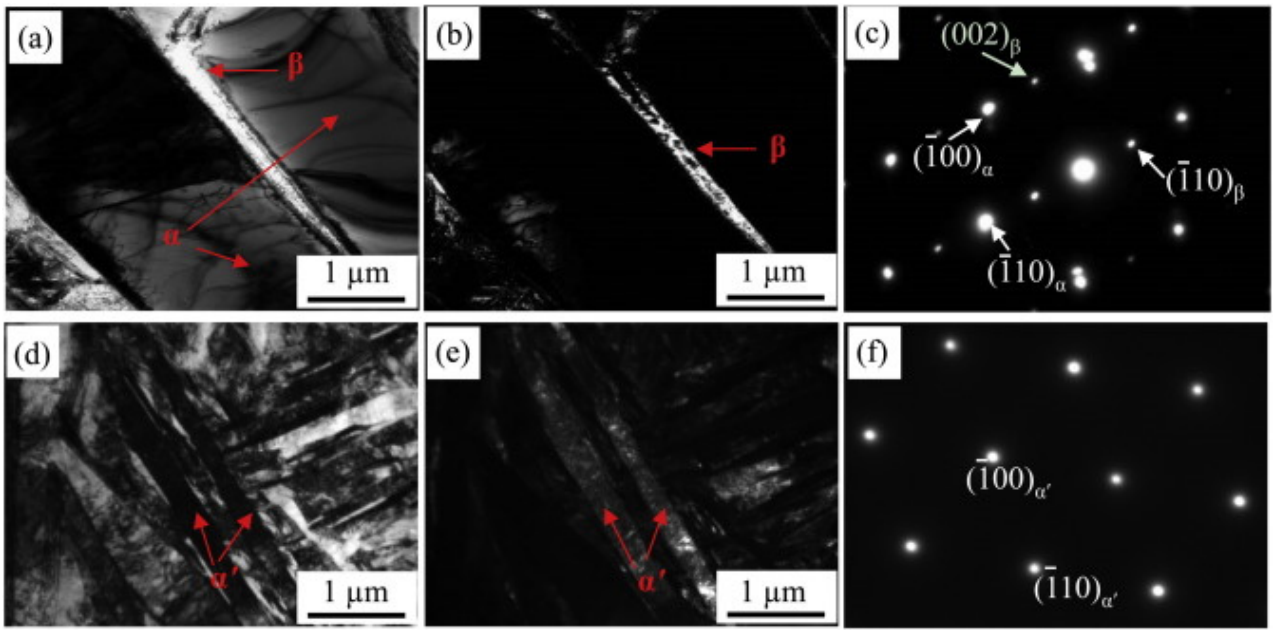

Figure 2. TEM images of Ti6Al4V produced by Electron Beam Melting (**a**–**c**) and LPBF (**d**–**f**): (**a**,**d**) bright-field images; (**b**,**e**) dark-field images; (**c**,**f**) diffraction patterns (reproduced with permission from [38]. Copyright 2016 Elsevier).

The TEM images given in Figure 2 show differences in the final microstructural features of Ti6Al4V produced by EBM and LPBF. In the EBM specimens, both body-centered cubic (bcc) and hexagonal close-packed (hcp) diffraction spots are observed, which confirms the existence of both the α and β phases. Additionally, it has to be mentioned that the thickness of the β phase is much thinner (~0.30 μm) than that of the α phase. Further, the volume fraction of β is quite low. On the other hand, in the Laser Powder Bed Fusion specimens, only the typical hcp diffraction spots are present, and the structure is fine α′ martensite [38], while in EBM specimens, both BCC (β phase) and HCP (α phase) phases are present, and these differences are explained by the higher cooling rate in the LPBF technique with respect to EBM. In general, lower substrate temperatures (≈200 °C) and an argon atmosphere are used for LPBF of Ti6Al4V-based components. These processing parameters lead to an

increased convective cooling rate compared to the higher substrate temperatures (≈450 °C) and vacuum atmosphere used in EBM [31,39]. The influence of each microstructural feature on the strength, ductility, hardness, fracture toughness, fatigue properties, wear resistance and corrosion behavior is meticulously addressed in the pertinent literature. The high strength [40], low weight ratio [41] and superior corrosion resistance of Ti6Al4V alloy make it suitable for a broad range of high-added-value products, from transportation and automotive industries [33] to chemical plants, oil and gas extraction, aerospace, medicine and aeronautics [31,32,42–44]. Table 1 lists the relevant physicomechanical properties of Ti6Al4V alloy and compares them with the properties of widely used materials in biomedical applications of cortical bone (i.e., CoCrMo alloys, 316 L stainless steel, and A357 aluminum alloy).

Table 1. Some physicomechanical properties of Ti6Al4V alloy, 316 L stainless steel, CoCrMo alloys, cortical bone, and A357 aluminum alloy [43,45–48].

Property	Stainless Steel 316 L (Cast)	F75 CoCrMo Alloy (Cast)	Cortical Human Bone	Ti6Al4V Alloy (Wrought)	Aluminium Alloy A357 (Cast)
Density (g/cm^3)	8.0	8.8	1.5–2	4.4	2.7
Yield strength (MPa)	205	500–1500	-	830–1070	265–275
Ultimate tensile strength (MPa)	515	900–1800	130–190	920–1140	331–351
Tensile modulus of elasticity (GPa)	195–205	200–230	10–30	100–110	70–75
Elastic elongation (%)	10–40	4–13	-	10–15	6

The attractive mechanical (i.e., lower Young´s modulus than cobalt alloys and stainless steels) and physical (i.e., low weight) properties of Ti6Al4V alloy, as well as its advantageous tribological (i.e., high corrosion resistance) and biological (i.e., excellent soft and hard tissue biocompatibility) performance, make this alloy very appealing for biomedical products such as orthopedic and dental implants [43,49–52]. With respect to aeronautics products such as engines (discs, blades and cooler parts), airframes, skins, flaps and slat tracks of wings and engine mountings, Ti6Al4V alloy is an appropriate choice, as it allows substantial weight savings and volume reduction compared to commonly used steels and aluminum. Additionally, this alloy presents good compatibility with composite materials allied to a high fatigue resistance and high-temperature mechanical properties [27,45].

3. Properties and Performance of Ti6Al4V Manufactured by LPBF

Laser Powder Bed Fusion provides very different mechanical properties from those of casting or wrought Ti6Al4V [9,53]. As highlighted in Figure 3, the inherent specificities of the LPBF process as a layer-by-layer building strategy, the powder feedstock, melting phenomena and thermal gradients will define the final properties, as they will dictate the microstructural features (e.g., grain size, crystal growth direction, residual porosity and defects, among others) [27,32,54,55].

Ti6Al4V suitability for a wide range of applications, particularly in industries such as aerospace and medical devices [39,56–59], is grounded in its material properties, especially when the strength-to-weight ratio and wear performance are key aspects. In this sense, this section is devoted to tensile properties and hardness (Section 3.1), fatigue behavior (Section 3.2) and wear performance (Section 3.3).

Table 2 provides a general outline of the latest studies on Ti6Al4V parts produced by LPBF, aiming to provide information regarding LPBF equipment specifications (and equipment manufacturing company) and the relevant properties being experimentally assessed. This table intends to help designers and manufacturers to quickly select the most effective approach for fabricating Ti6Al4V parts using a given type of equipment.

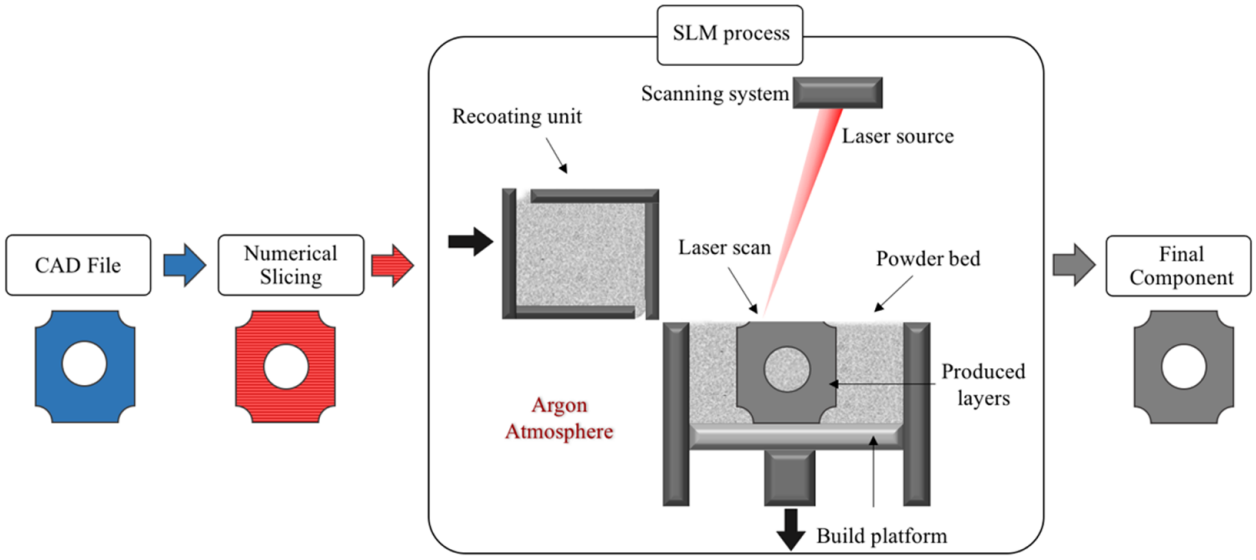

Figure 3. Schematic representation of Laser Powder Bed Fusion technology.

Table 2. Summary of studies addressing Ti6Al4V parts produced by LPBF.

Company	SLM Solutions GmbH (Germany)				EOS GmbH (Germany)		Concept Laser GmbH (Germany)	Renishaw (UK)
Equipment	SLM 125HL [60]	SLM 250HL	SLM 280HL [61]	EOSINT M270	EOSINT M280 [62]	EOSINT M290 [63]	M2 cusing [64]	AM 250
Build Envelope (mm^3)	125 × 125 × 125	-	280 × 280 × 365	250 × 250 × 215	250 × 250 × 325	250 × 250 × 325	250 × 250 × 280	250 × 250 × 300
Laser details	IPG fiber laser 400W	IPG fiber laser 400W	IPG fiber laser 400, 700 or 1000W	Yb-fiber laser 200W	Yb-fiber laser 200 or 400W	Yb-fiber laser 400W	Fiber laser 200 or 400W	Yb-fiber laser 200W
Tensile strength	[33,65]	[56,66,67]	[68]	[69–71]	[21,72–75]	[76–78]	[55]	[79–81]
Tensile strain	[33,65]	[56,66,67]	[68]	[69–71]	[21,72–74]	[76,77]	[55]	[79–81]
Young's Modulus	[33]	-	[82]	[69,83]	[72]	[77]		[79]
Fatigue behavior	-	[4,41,56,84–86]	[85]	[7,69,70]	[21,72,74,87]	[77,78]	[55]	
Fatigue crack analysis	-	[4,56,84–86,88]	[85]	[7,69–71]	[72,74]	[77]	[55]	
Hardness	[2,3]	[86]	-	[69]	[89]	[90]		[80]
Density	[2,3]	[31,66]	-	[83,91,92]	[89]	[77]	[55,93]	[81]
Microstructure	[3,33,94]	[56,66,67,84,95]	[68,82]	[7,69–71,83,92]	[21,72,73,75,89]	[76,78,96]	[55]	[81,97,98]
Heat treatments		[4,56,67,84–86]	[68,85]		[21,72,73,75]	[77]		[80]
Parameters assessment	[3,65]	[31,66]	-	[69,92]		[90]	[55,93]	[81]
Surface roughness			-		[73,74,96]	[90,96]		

3.1. Tensile Properties

The consolidation of the metal powder by LPBF is achieved by the temperature effect (laser as the energy source for melting), gravity and capillary forces [55,99]. Due to the large number of influential processing parameters on layer-by-layer AM processes, the production of high-quality Ti6Al4V parts having high densification requires complete control of the process [3,56,100]. Most of the published studies on Ti6Al4V manufactured by LPBF report near full density and superior strength to that obtained when using conventional processing routes (such as cast or wrought) [66]. Nevertheless, it should be highlighted that a proper assessment of the most suitable processing parameters is very relevant [34,101,102] for each piece of Laser Powder Bed Fusion equipment used in the fabrications, as the density of energy is not a sufficient parameter to optimize the processing parameters, as shown in Figure 4. In fact, several studies have been devoted to the assessment of the effects of LPBF processing parameters on several physical and mechanical properties, correlating them with the microstructure, defect generation, etc. [3,31,55,69,103]. A summary of the tensile properties of Ti6Al4V parts produced by LPBF is found in Table 3.

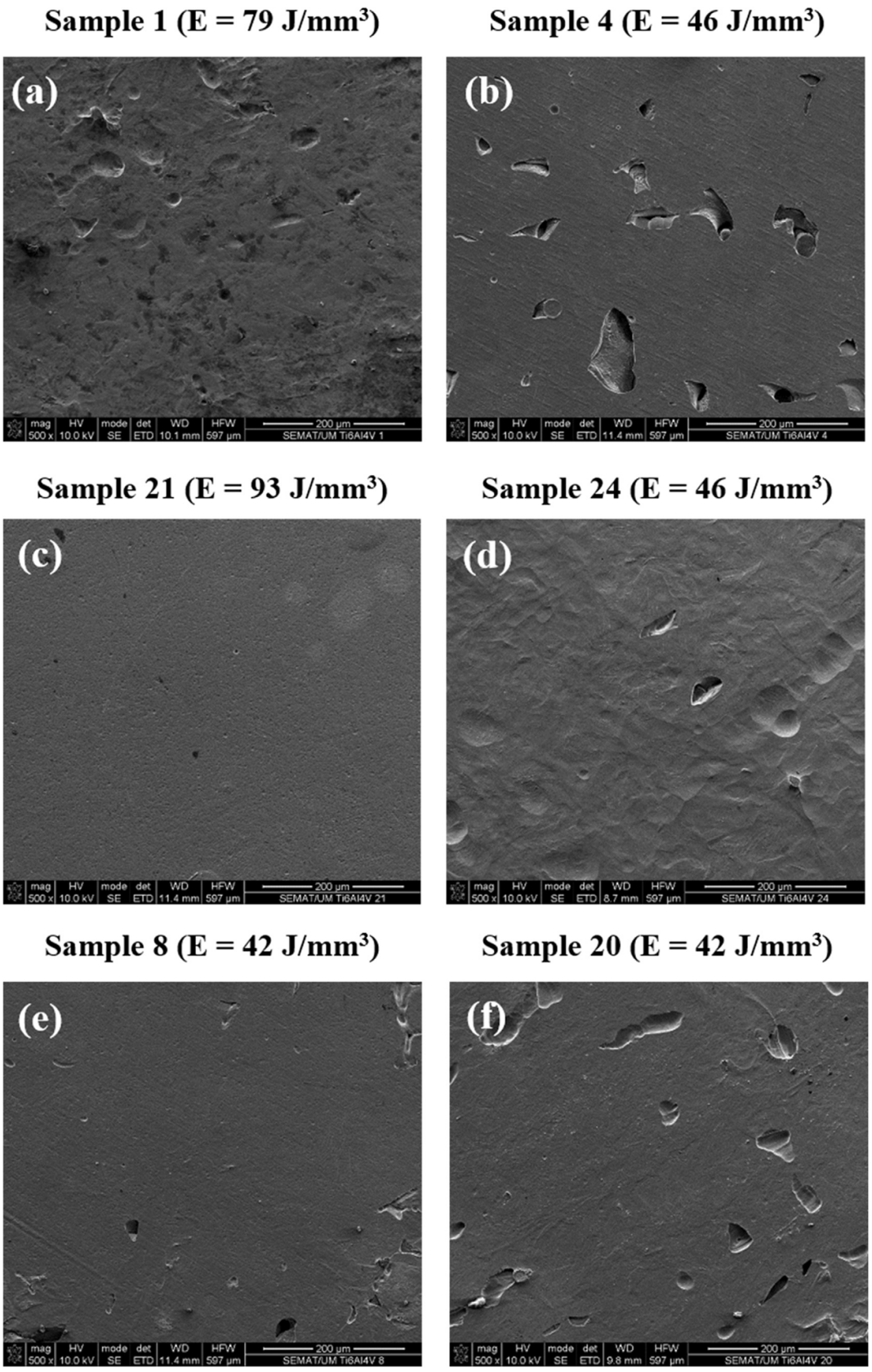

Figure 4. SEM images of Ti6Al4V fabricated by LPBF using different densities of energy (reproduced with permission from [3]. Copyright 2016 Elsevier).

Table 3. Tensile properties of LPBF Ti6Al4V, indicating the testing direction with respect to the building direction.

Reference	Yield Strength (MPa)	Tensile Strength (MPa)	Tensile Strain (%)	Young's Modulus (GPa)	Direction
Benedetti et al. [104]	1015	1090	10	113	-
Shunmugavel et al. [33]	964	1041	7	113	*longitudinal*
	1058	1114	3	109	*transversal*
Vandenbroucke et al. [105]	1125	1250	6	93	-
Vrancken et al. [106]	1110	1267	7.3	109	*transversal*
Edwards et al. [41]	910	1035	3	-	*transversal*
Vilaro et al. [58]	1137	1206	7.6	105	*longitudinal*
	962	1166	1.7	102	*transversal*
Koike et al. [107]	850	960	6.8	-	-
Anatoliy et al. [68]	1200	1280	2.4	-	-
Gong et al. [69]	1098	1237	8.8	109	-
Leuders et al. [56]	1008	1080	1.6	-	-
Wysocki et al. [108]	1150	1246	1.4	-	*longitudinal*
	1273	1421	3.2	-	*transversal*
Kasperovich et al. [55]	802	1062	12.7	-	*longitudinal*
Rafi et al. [71]	1195	1269	5	-	*longitudinal*
	1143	1219	4.9	-	*transversal*
Mower et al. [72]	972	1034	-	109	*longitudinal*
	1096	1130	-	115	*transversal*
Huang et al. [80]	970	1191	5.4	-	-
Fachini et al. [100]	990	1095	8.1	110	-

Considering the standards for Ti6Al4V alloy for surgical implants and for aerospace applications (e.g., ASTM F136–13; ASTM F1108–14; AMS4930; AMS6932), the minimum values for tensile properties can be defined as follows: yield strength of 758 MPa, tensile strength of 827 MPa and tensile strain of 8%. LPBF Ti6Al4V displays superior yield and tensile strength to those of cast or wrought alloy, mainly due to microstructural features such as grain refinement [66]. On the contrary, when regarding tensile strain, Ti6Al4V fabricated by LPBF exhibits lower ductility when compared to cast or wrought [53]. As depicted in Table 3, several studies on LPBF Ti6Al4V parts show yield and tensile strengths that are significantly higher compared to the ASTM specification [33,41,53,72,106]; however, when regarding tensile strain, most of the studies report values lower than the minimum required (10%). This aspect is mainly the reason why heat treatments are usually performed on Ti6Al4V alloy fabricated by LPBF.

The Ti6Al4V alloy microstructure is dependent on the thermal history occurring during the fabrication but can be defined by post-processing heat treatments. Table 4 and Figure 5 show that different heat treatments (selected temperatures and cooling rates) induce substantial differences in the microstructural features of LPBF Ti6Al4V alloy in comparison to the as-built LPBF alloy and the ensuing mechanical properties [55,58,80,106].

The mechanical properties of Ti6Al4V are dictated by its microstructure, particularly by the constituent phases (α', α and β) and grain size [54,109,110]. Typically, Ti6Al4V alloy exhibits a microstructure that ranges from lamellar to globular [67,77,111]. While the first is usually desirable for enhanced fracture toughness, globular microstructure displays, on average, superior tensile strength and ductility [21]. A typical equiaxed microstructure with a globular α phase in an $\alpha + \beta$ matrix is observed in wrought Ti6Al4V alloy [29]. This microstructure typically leads to tensile strengths ranging from 897 to 984 MPa and tensile strains ranging from 10 to 19% [53,55,112,113].

Table 4. Overview of the microstructure and mechanical properties before and after heat treatments on LPBF Ti6Al4V: YS = yield strength; TS = tensile strength; TS′ = tensile strain; WQ = water quenching (>410 °C/s); AC = air cooling; FC = furnace cooling.

Reference	Condition/Heat Treatment	YS (MPa)	TS (MPa)	TS′ (%)	Microstructure
Kasperovich et al. [55]	Wrought	927	984	19.3	globular α + β (Figure 1a)
	As-built	736	1051	11.9	α′ acicular, column width < 0.5 µm (Figure 1b)
	700 °C–1 h–FC (10 °C/min)	1051	1115	11.3	α′ acicular, column width < 1.0 µm (Figure 1c)
	900 °C–2 h followed by 700 °C–1 h–FC (10 °C/min)	908	988	9.5	elongated primary α grains in a β matrix (Figure 1d)
	HIP (900 °C/100 MPa–2 h) followed by 700 °C–1 h–FC (10 °C/min)	885	973	19	elongated primary α grains in a β matrix (Figure 1e)
Vilaro et al. [58]	As-built	1137	1206	7.6	α′ acicular (Figure 2a)
	730 °C–2 h–AC	965	1046	9.5	α′ acicular embedded in α + β phases (Figure 2b)
	950 °C–1 h–WQ	944	1036	8.5	α′ acicular, α and β (Figure 2c)
	1050 °C–1 h–WQ	913	1019	8.9	α′ acicular (Figure 2d)
Huang et al. [80]	As-built	970	1191	5.4	α′ acicular (Figure 3a)
	800 °C–2 h–AC	1010	1073	17.1	less fine α′ acicular embedded in α + β phases (Figure 3b)
	950 °C–2 h–AC	893	984	14.2	α laths in β matrix (Figure 3c)
	1050 °C–1 h–AC	869	988	13.3	equiaxed and α-equiaxed prior β grains (Figure 3d)
	1200 °C–1 h–AC	897	988	11.3	α-equiaxed prior β grains
Vrancken et al. [106]	Forged	960	1006	18.4	α + β
	As-built	1110	1267	7.3	α′ acicular (Figure 4a)
	540 °C–5 h–WQ	1118	1223	5.4	-
	850 °C–2 h–FC (0.04 °C/s)	988	1004	12.8	α′ acicular, α and β (Figure 4b)
	940 °C–1 h–AC followed by 650 °C–2 h–AC	899	948	13.6	long columnar prior β grains (Figure 4c)
	1015 °C–0.5 h–AC followed by 730 °C–2 h–AC	822	902	12.7	-
	1015 °C–0.5 h–AC followed by 843 °C–2 h–FC (0.04 °C/s)	801	874	13.5	α + β
	1020 °C–2 h–FC (0.04 °C/s)	760	840	14.1	α + β (Figure 4d)
Leuders et al. [56]	As-built	1008	1080	1.6	α′ acicular
	800 °C–1h–FC	962	1040	5	α′ acicular, α + β
	1050 °C–1 h–FC	798	945	11.6	α + β
	HIP (920 °C/1000 bar)–2 h–FC	912	1005	8.3	α + β

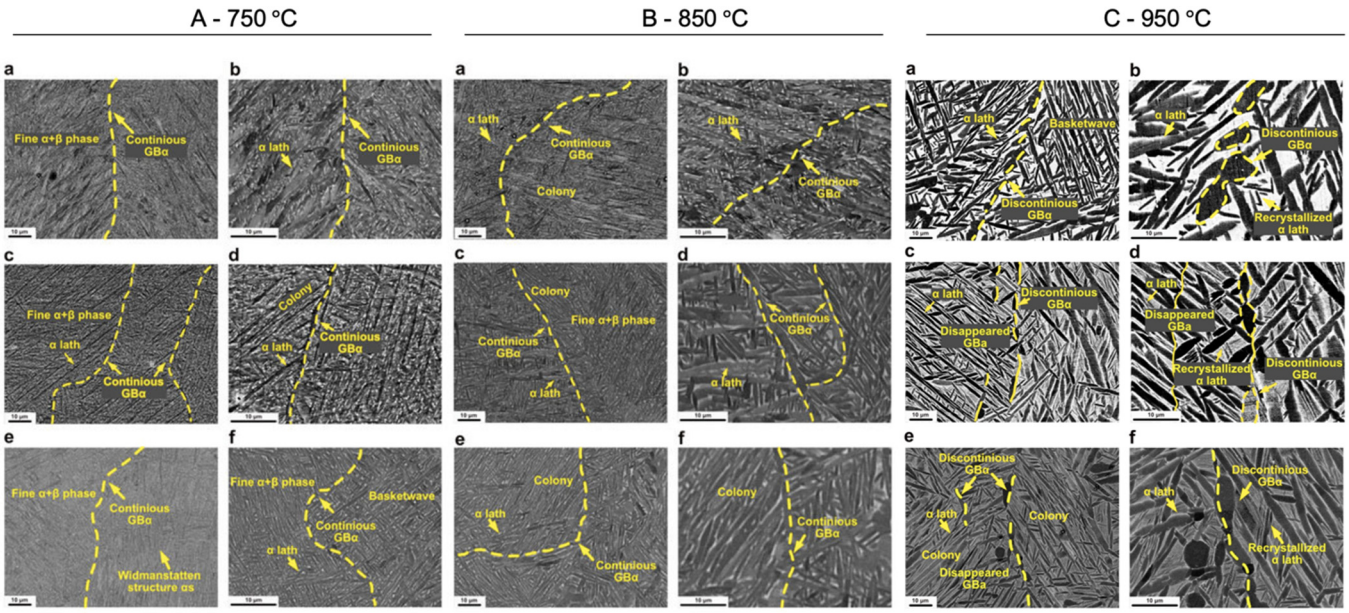

Figure 5. Microstructures of Ti6Al4V parts produced by LPBF with different heat treatments: (**a**,**b**) heat stage followed by water quenching; (**c**,**d**) heat stage followed by air cooling; (**e**,**f**) heat stage followed by furnace cooling (adapted with permission from [5]. Copyright 2021 Emerald Publishing Limited).

During LPBF fabrication, this alloy undergoes extremely high cooling rates (10^3–10^8 K/s), resulting in an acicular martensite phase known as the α' phase [54,114,115]. Consequently, the as-built LPBF Ti6Al4V microstructure evidences a needle-like morphology, as shown in Figures 1c and 2a [55,77,80,106]. Several heat treatments have been reported in the literature, mostly performed to increase the low ductility displayed by LPBF Ti6Al4V by promoting significant microstructural changes. When observing Figure 5, it is possible to conclude several aspects. In this heat treatment, the α' martensite can decompose into an α + β phase, along with the formation of GB-α, and the thickness of the α lath after sub-transus heat treatment (HT) is primarily dependent on the maximum HT temperature and the cooling rate. In addition, the morphology of GB-α is mainly dependent on the HT temperature, and the GB-α exhibits a discontinuous morphology when HT temperatures increase to nearly the β transus (950 °C). It can be highlighted that for heat treatments below the β transus (≈950 °C) [5], β transformation occurs, with the cooling rate dictating the final phases, and even when the same phase is attained, their shape and size (e.g., α plate width) are also ruled by the cooling velocity [54,58,106,116]. When performing a heat treatment below the β transus temperature, a coarsening of the acicular martensite occurs, with larger lamellae when compared to the as-built alloy. Figure 5A,B evidence this phenomenon for heat treatments performed at 750 and 850 °C, respectively. Figure 5C shows that when performing a heat treatment of 950 °C, an elongated primary α grain in a β matrix is observed. Considering heat treatments above the β transus, again, the cooling rate defines the final microstructure: typically, furnace cooling creates a lamellar α + β structure, air cooling leads to an α-Widmanstatten structure, and water quenching (>410 °C/s) leads to an α' martensite structure or fine, fine α lath [116]. As an example, Figure 5C shows a microstructure with α laths in a β matrix, which demonstrates that when performing a heat treatment above the β transus (950 °C) followed by air cooling, α' acicular is no longer present. For this same example, Table 4 shows that this change in microstructure led to a decrease in the tensile strength (from 1191 to 984 MPa), while tensile strain was enhanced from 5.4 to 14.2%.

3.2. Fatigue Behavior

The fatigue performance is the response of a material to repeated cyclic loads and/or strains, and the fatigue strength dictates whether a certain material under continuous cyclic stresses is capable of ensuring a long operating life [117]. Components under cyclic loading are rather common in a variety of structures and equipment, and for that reason, fatigue failure is one of the most common failure modes [27]. The fatigue performance is crucial for load-bearing medical implants and for aerospace components [41,118].

The assessment of the fatigue performance usually comprises three different approaches: stress-based (S-N), strain-based (ε-N) or fracture mechanisms, in which N represents the number of cycles before failure. As seen in Figure 6, the evolution of a fatigue crack progresses through three main regions, starting with crack initiation, followed by crack propagation and, lastly, the fracture [119]. Crack initiation is difficult to detect and sensitive to the size of the microstructural grain (REF). In fact, finer grains lead to the closer spacing of grain boundaries, which the crack has to break through, delaying crack initiation. On the other hand, crack propagation (Region II in Figure 6) is not influenced by the microstructure, being better described by a power law such as Paris's law [119].

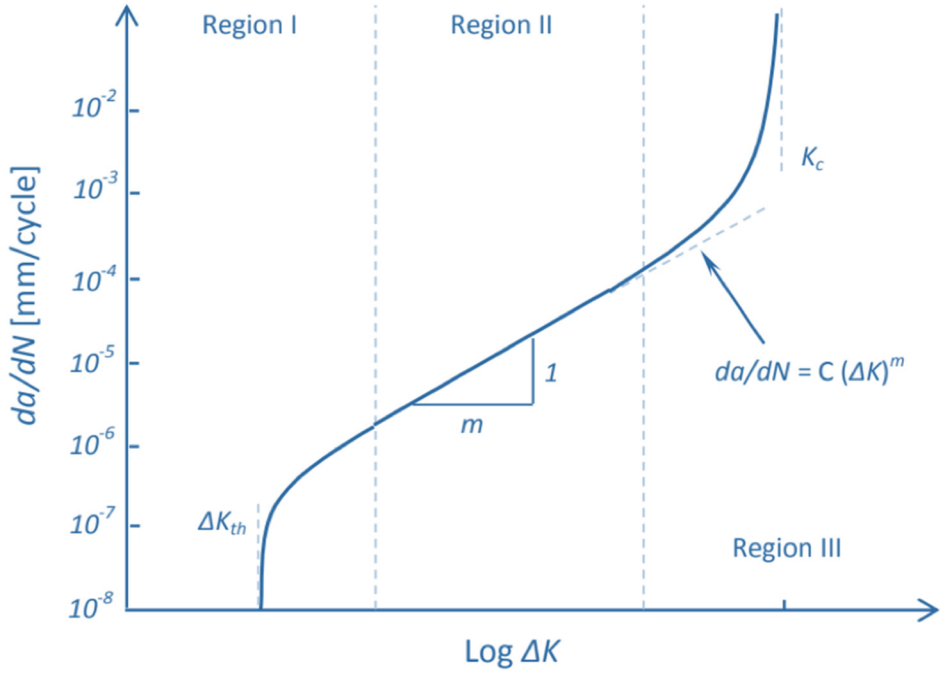

Figure 6. Fatigue crack propagation regimes.

The crack propagation threshold, ΔK_{th} (MPa$\sqrt{m}$), the Paris slope, the fracture toughness (K_c (MPa$\sqrt{m}$) and the number of cycles before failure can be assumed as the main parameters to assess the fatigue behavior of a material. Table 5 summarizes this fatigue data for as-built and post-treated Ti6Al4V alloy fabricated by LPBF.

LPBF processing parameters are one crucial aspect that dictates the fatigue performance of Ti6Al4V alloy produced by this technology [69,84,121]. When considering the role of processing parameters on the quality of Ti6Al4V parts fabricated by LPBF, two types of defects are commonly described. The first is the incomplete powder melting or improper fusion between successive tracks or layers caused by insufficient energy input. The second occurs with the entrapment of gases due to excessive energy. Regarding the influence of LPBF processing parameters on the fatigue performance of Ti6Al4V, Gong et al. [69] studied five processing conditions, varying the scan speed (see Figure 7) to obtain five different energy densities (from 27 to 100 J/mm^3). The results showed that when using 42 and 74 J/mm^3, comparable fatigue life limits (≈350 MPa for 10^7 cycles) were obtained, with the highest being among the tested conditions. Specimens fabricated using 100 J/mm^3

exhibited pores with larger sizes and numbers (higher porosity) than those in the previously mentioned conditions, consequently displaying a lower fatigue life (300 MPa). Finally, for the lowest energy densities (27 and 32 J/mm^3), the presence of lack-of-fusion defects seriously compromised the fatigue performance (fatigue limit of 100 MPa).

Table 5. High cycle fatigue properties of LPBF Ti6Al4V, indicating the testing direction with respect to the building direction (for a stress ratio of 0.1).

Reference	*Condition/Heat Treatment*	Δk_{th} *(MPa$\sqrt{m}$)*	*m (Paris Slope)*	K_c *(MPa$\sqrt{m}$)*	*Fatigue Limit*	*Microstructure*	*Direction*
Gong et al. [69]	As-built (OP1)	-	-	-	10^7 cycles for 350 MPa	α' acicular	-
	As-built (MP2)	-	-	-	10^7 cycles for 350 MPa	α' acicular	-
	As-built (MP3)	-	-	-	10^7 cycles for 300 MPa	α' acicular	-
	As-built (MP4)	-	-	-	10^7 cycles for 100 MPa	α' acicular	-
	As-built (MP5)	-	-	-	10^7 cycles for 100 MPa	α' acicular	-
Leuders et al. [56]	As-built	1.7	-	-	-	α' acicular	*longitudinal*
	800 °C–1 h–FC	3.7	-	-	-	α' acicular, α + β	*longitudinal*
	1050 °C–1 h–FC	6.1	-	-	-	α + β	*longitudinal*
	HIP (920 °C/1000 bar)–2 h–FC	≈3.7	-	-	-	α + β	*longitudinal*
	As-built	1.4	-	-	2700 cycles for 600 MPa	α' acicular	*transversal*
	800 °C–1 h–FC	3.9	-	-	93,000 cycles for 600 MPa	α' acicular, α + β	*transversal*
	1050 °C–1 h–FC	3.9	-	-	2.9×10^4 cycles for 600 MPa	α + β	*transversal*
	HIP (920 °C/1000 bar)–2 h–FC	≈4.0	-	-	2×10^6 cycles for 600 MPa	α + β	*transversal*
Riemer et al. [85]	As-built	1.4	-	-	-	-	-
	800 °C–2 h–FC	3.9	-	-	-	-	-
	1050 °C–2 h–FC	3.6	-	-	-	-	-
	HIP (920 °C/1000 bar)–2 h–FC	4.2	-	-	-	-	-
Greitemeier et al. [21]	As-built (710 °C–2 h–Argon cooling)	≈3.0	-	-	1×10^7 cycles for 200 MPa	α' acicular	-
	Milled (710 °C–2 h–Argon cooling)	≈3.0	-	-	1×10^7 cycles for ≈460 MPa	α' acicular	-
	As-built (HIP (920 °C/1000 bar)–2 h)	≈4.0	-	-	1×10^7 cycles for ≈150 MPa	α + β	-
	Milled (HIP (920 °C/1000 bar)–2 h)	≈4.0	-	-	1×10^7 cycles for ≈600 MPa	α + β	-
Rafi et al. [120]							
Wycisk et al. [70]	As-built (650 °C–3 h–Argon cooling)	-	-	-	10^7 cycles for 210 MPa	α' acicular	*longitudinal*
	Polished (650 °C–3 h–Argon cooling)	-	-	-	10^7 cycles for 510 MPa	α' acicular	*longitudinal*
	Shot-peened (650 °C–3 h–Argon cooling)	-	-	-	10^7 cycles for 435 MPa	α' acicular	*longitudinal*
Edwards et al. [88]	As-built	6.3	2.612	72.8	-	α' acicular	*longitudinal*
	As-built	5.8	2.366	70.1	-	α' acicular	*transversal*
	As-built	5.9	2.451	43.4	-	α' acicular	*transversal*

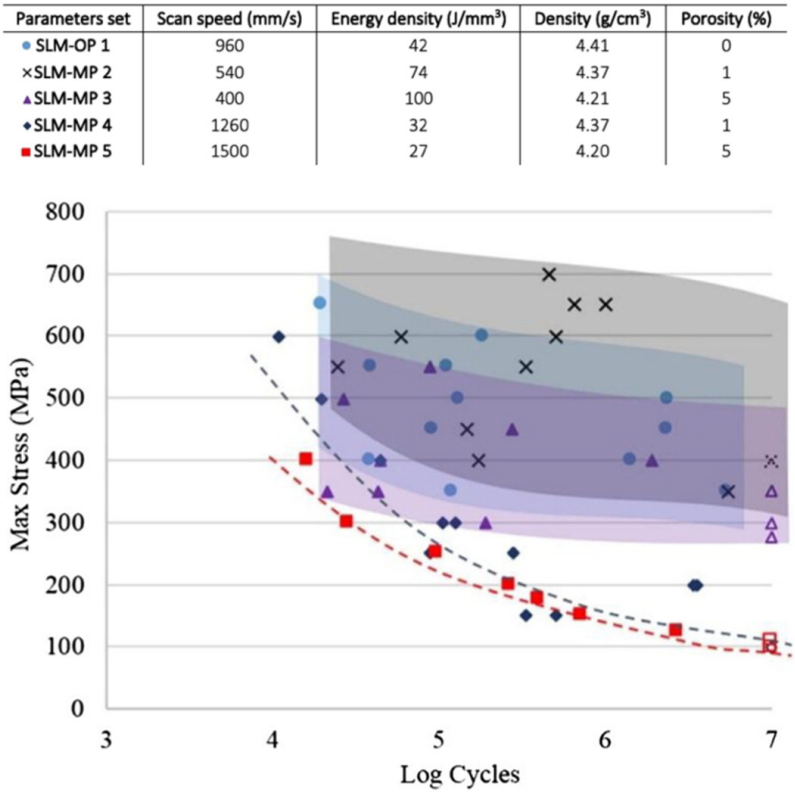

Figure 7. Fatigue life of LPBF Ti6Al4V specimens produced with different processing conditions (adapted with permission from [69]. Copyright 2015 Elsevier).

The microstructure of Ti6Al4V alloy is another aspect when thinking about fatigue performance, and several studies have reported the influence of thermal and thermo-mechanical treatments on the fatigue behavior of this alloy [21,56,85]. As an example, Leuders et al. [56] showed that heat treatments have a strong influence on the fatigue behavior of LPBF Ti6Al4V parts. In their study, while the fatigue life for as-built Ti6Al4V was 27,000 cycles, after performing heat treatments at 800 °C (below β transus) or 1050 °C (above β transus), this number was respectively increased to 93,000 or 290,000 cycles (for a stress amplitude of 600 MPa). After performing a thermo-mechanical treatment (HIP), none of the specimens fractured before 2×10^6 cycles, showing the ability of this thermo-mechanical treatment to improve the fatigue life of LPBF Ti6Al4V through a reduction in detrimental internal defects.

S. Leuders et al. [56] showed that as-built Ti6Al4V has a crack growth behavior at a lower crack growth rate, which is similar in both directions. As detected for the fatigue life, a significant enhancement of the crack propagation threshold (ΔK_{th}) is observed when performing thermal or thermo-mechanical treatments on as-built Ti6Al4V, as proven by the evident shift of the curves to the right. This trend was verified in specimens tested perpendicular or parallel to the build direction.

Another work from Riemer et al. [85] confirmed the effect of thermal and thermo-mechanical treatments on the fatigue behavior of as-built LPBF Ti6Al4V. As seen in Figure 8, the results are aligned with those from Leuders et al. [56], with the as-built LPBF Ti6Al4V showing low and insufficient fatigue performance. Moreover, heat treatments at 800 °C, 1050 °C and HIP also lead to a significant improvement, with higher crack propagation threshold values (3.9, 3.6 and 4.2 MPa $\sqrt{m}$, respectively) when compared to the as-built condition (1.4 MPa $\sqrt{m}$) [85] (see Figure 8).

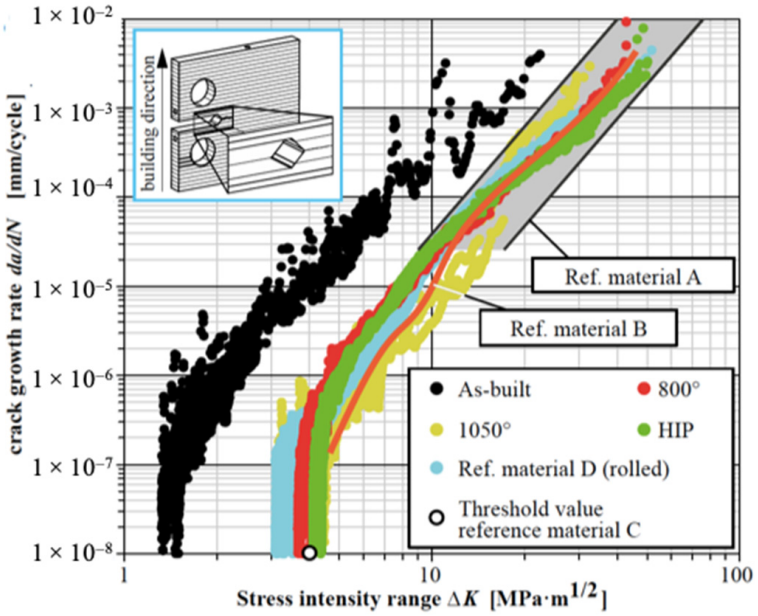

Figure 8. Fatigue crack growth data of Ti6Al4V by LPBF for different material conditions (building direction is normal to crack growth direction (reproduced with permission from [85]. Copyright 2016 Andre Riemer).

The surface condition is a key aspect that has a huge impact on the fatigue performance of Ti6Al4V alloy produced by LPBF [21,69,74]. Being a powder-bed fusion technique, LPBF displays an inherent surface condition for Ti6Al4V. As shown in Figure 9, LPBF induces the presence of two types of roughness, a primary roughness resulting from the solidification of the melt pool and a second one due to partially melted powder particles ($R_a \approx 13$ μm) [74].

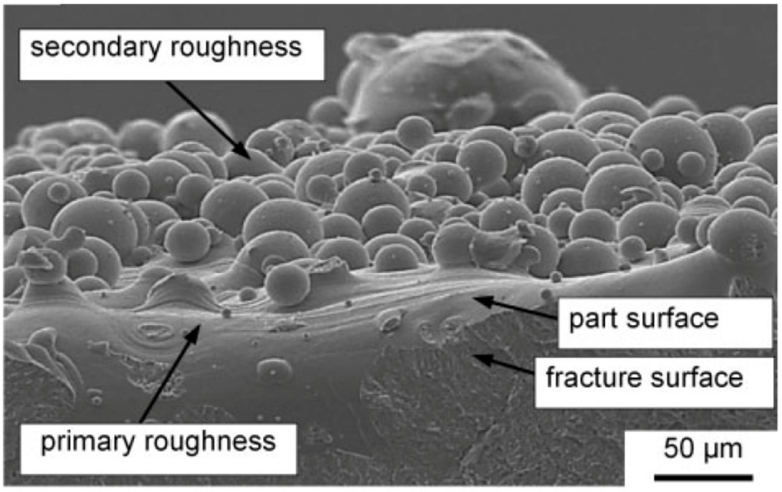

Figure 9. Typical surface roughness of Ti6Al4V produced by Laser Powder Bed Fusion.

On this subject, Greitemeier et al. [21] reported the fatigue performance of LPBF Ti6Al4V specimens, as-built and milled (see Figure 10), also addressing the influence of thermal and thermo-mechanical treatments on the fatigue behavior. From their results, it is possible to conclude that, independently of the heat treatment, the fatigue life of milled LPBF specimens is superior to that of as-built specimens. As reported elsewhere [21,74,111,122], Greitemeier et al.'s [21] study highlights the detrimental effect of LPBF's inherent surface condition (see Figure 11) on the fatigue performance of this alloy. When comparing as-built and milled specimens subjected to thermal or thermo-mechanical treatments, significant differences in fatigue life stress limits were found. For annealed specimens, an improvement in the fatigue stress limit of 2.4 times was observed when changing the surface condition from as-built to milled. Similarly, for HIP specimens, an enhancement of 3.4 times was obtained by performing milling.

The high impact of the surface condition on the fatigue behavior of LPBF Ti6Al4V was also reported by Gong et al. [69]. These authors compared LPBF parts fabricated using very dissimilar processing energy densities (from 32 to 74 J/mm^3), and although leading to significantly different fatigue limits, similar crack initiations were found, all at surface or sub-surface defects, as shown in Figure 11.

In sum, the fatigue properties of Ti6Al4V alloy produced by Laser Powder Bed Fusion are dictated by three main aspects:

(1) **The densification level** of the produced parts, which is defined by the processing parameters used in the fabrication. When defects such as pores and lack of fusion are present in higher amounts (porosity higher than 5%), the fatigue performance tends to be poor [4,69]. In this scenario, cracks can initiate either in the bulk or at the surface due to these defects [84].

(2) **The microstructural features** are another important aspect because by performing thermal and thermo-mechanical post-treatments, it is possible to substantially improve the fatigue performance of this alloy by altering its microstructure. Hot Isostatic Pressing (a thermo-mechanical treatment) proves to be the most effective post-treatment to increase the fatigue performance of LPBF Ti6Al4V [4,21,84]

(3) **The surface condition** has a crucial impact on the fatigue performance of this alloy, and regarding LPBF, the natural surface condition was found to be extremely detrimental, even when performing post-treatments on LPBF as-built parts (see Figure 10). In this sense, machining LPBF as-built parts seem to be an effective way to enhance the fatigue performance of Ti6Al4V parts manufactured by this technology.

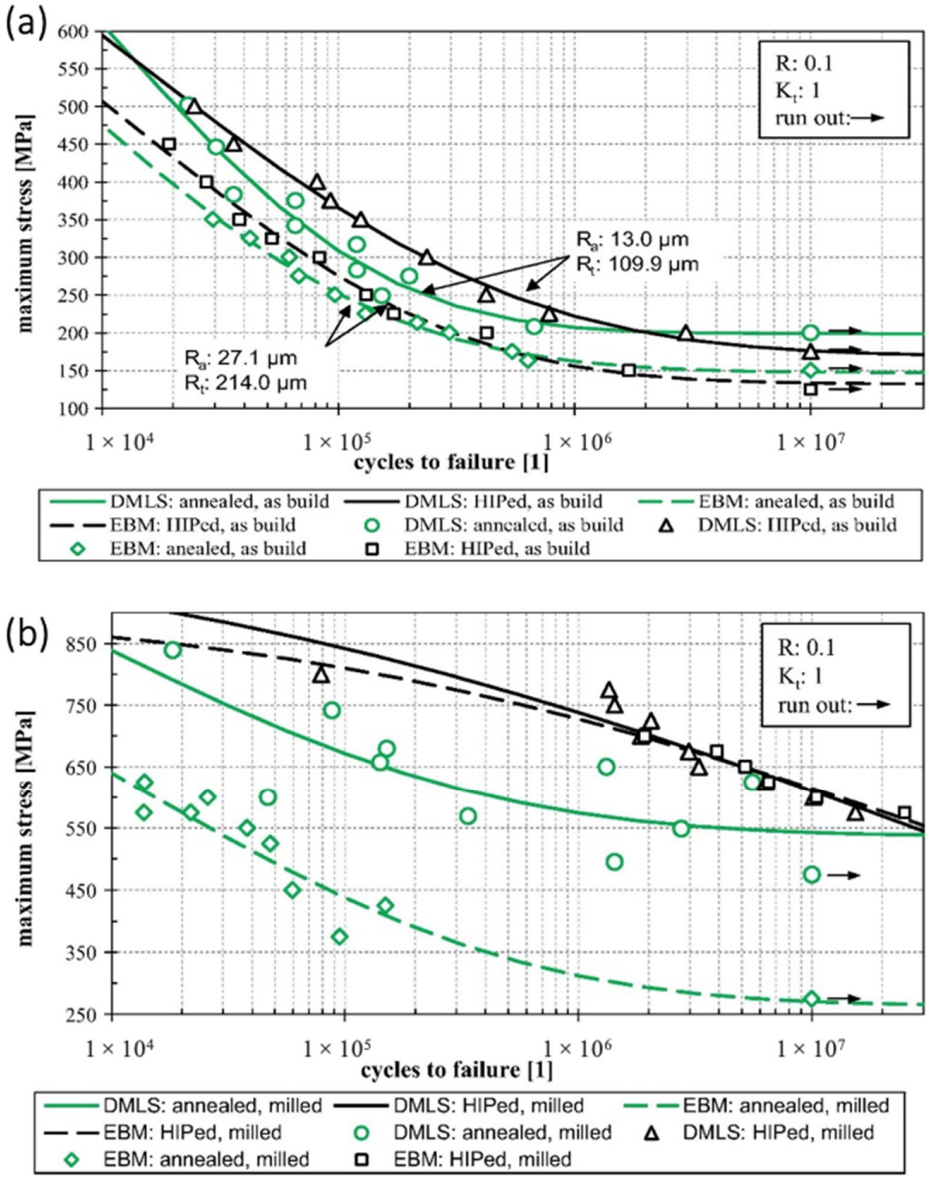

Figure 10. Fatigue properties of Ti6Al4V by LPBF and EBM for (**a**) as-built and (**b**) milled surfaces (adapted with permission from [21]. Copyright 2016 Elsevier).

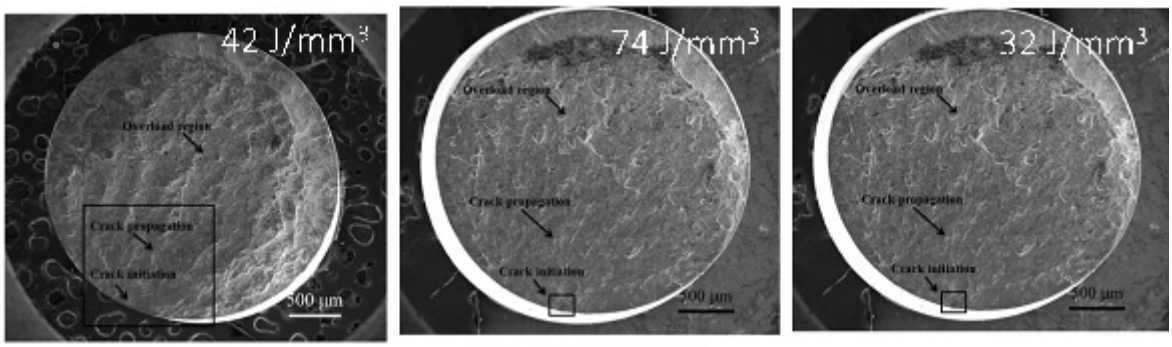

Figure 11. Fracture surfaces of Ti6Al4V by LPBF using different processing conditions corresponding to energy densities of 42, 74 and 32 J/mm^3 (adapted with permission from [69]. Copyright 2015 Elsevier).

3.3. Hardness and Wear Performance

The data found in the literature for the hardness of Ti6Al4V alloy produced by LPBF show higher values when compared to those of wrought alloy (314 HV) [3,55,123,124]. This fact is explained by the inherent microstructure that LPBF induces in Ti6Al4V due to the typical high cooling rate (10^3–10^8 K/s). As-built LPBF Ti6Al4V alloy exhibits an acicular microstructure (α' phase), which is a harder phase when compared to the α and β phases present on the wrought alloy [125,126].

As previously mentioned for strength, heat treatments also influence the hardness of this alloy due to changes in the microstructural phases. Depending on the heat treatment temperature and cooling rate, it is possible to change the full acicular microstructure (α') of as-built LPBF Ti6Al4V to a coarser acicular microstructure; to an acicular α' mixed with $\alpha + \beta$ microstructure; or even to an $\alpha + \beta$ microstructure (absent α' phase). These differences in the microstructure, as reported by Kasperovich et al. [55], result in higher hardness for the as-built condition (360 HV) when compared to the alloy after heat treatments performed at 700 °C (351 HV) and 900 °C (324 HV).

Typically, LPBF Ti6Al4V in the as-built condition exhibits higher tensile strength, lower ductility and higher hardness, while after performing post-treatments (thermal), lower tensile strength, higher ductility and lower hardness are generally attained (see Tables 3 and 5). Table 6 presents an overview of the hardness values found in the literature for LPBF Ti6Al4V, either as-built or after thermal treatments [3,55,107,123].

Table 6. Summary of LPBF Ti6Al4V hardness data extracted from literature.

Reference	Condition/Heat Treatment	Hardness (HV)	Microstructure
Kasperovich et al. [55]	Wrought	314	$\alpha + \beta$ globular
	As-built	360	α' acicular
	700 °C–1 h–FC	351	α' acicular
	900 °C–2 h followed by 700 °C–1 h–FC	324	α grain in β matrix
Koike et al. [107]	As-built	≈400	α' acicular
Kruth et al. [123]	As-built	380–420	α' acicular
Bartolomeu et al. [3]	As-built	389	α' acicular
Li et al. [120]	As-built	≈400	-
Amaya-Vazquez et al. [127]	As built	440	α' acicular
Song et al. [124]	As-built	450	-
Vilaro et al. [58]	As-built	354	α' acicular
	730 °C–2 h–AC	344	α' acicular, $\alpha + \beta$

The wear performance of a material is usually correlated to its hardness; i.e., higher hardness leads to a higher wear performance [29]. To the authors' knowledge, there are a very limited number of studies on the wear performance of Ti6Al4V alloy or pure titanium produced by LPBF [110,128,129]. Kumar and Kruth [129] showed that LPBF Ti6Al4V exhibited the lowest fretting wear performance when compared to stainless steels, tool steel and a cobalt–chrome alloy, but the comparison was made between LPBF Ti6Al4V and this same alloy fabricated by different routes. Gu et al. [110] studied the wear behavior of commercially pure titanium fabricated by LPBF using four different processing parameters. Their results show an inversely proportional relationship between the nanohardness and the wear rate for all processing conditions. The processing parameters that led to the highest hardness value (≈4 GPa) were the same that were used for fabricating the material that exhibited the highest wear performance (lowest wear rate $\approx 7 \times 10^{-4}$ mm^3/N·m). These authors also reported that the wear performance of this material produced by LPBF was higher than that of the reference material fabricated by powder metallurgy due to the presence of a refined α' acicular microstructure [110].

Bartolomeu et al. [2] studied the wear performance of Ti6Al4V produced by LPBF, comparing it with hot-pressed and cast Ti6Al4V. Figure 12 shows the overall results of this study showing the interrelation between the microstructure, the hardness and the wear

rate for the three different processing routes investigated. Figure 12 shows that the highest wear performance (lowest wear rate ≈ 6.5×10^{-4} $mm^3/N{\cdot}m$) was observed for the LPBF alloy, which displayed the highest hardness (≈388 HV). On the other hand, the lowest wear performance (highest wear rate ≈ 8.3×10^{-4} $mm^3/N{\cdot}m$) was detected for cast Ti6Al4V, which had the lowest hardness (≈342 HV). Considering that these three materials (cast, HP and LPBF) were almost fully densified, these authors stated that the wear performance is explained by the microstructural features and the resulting hardness [125,126].

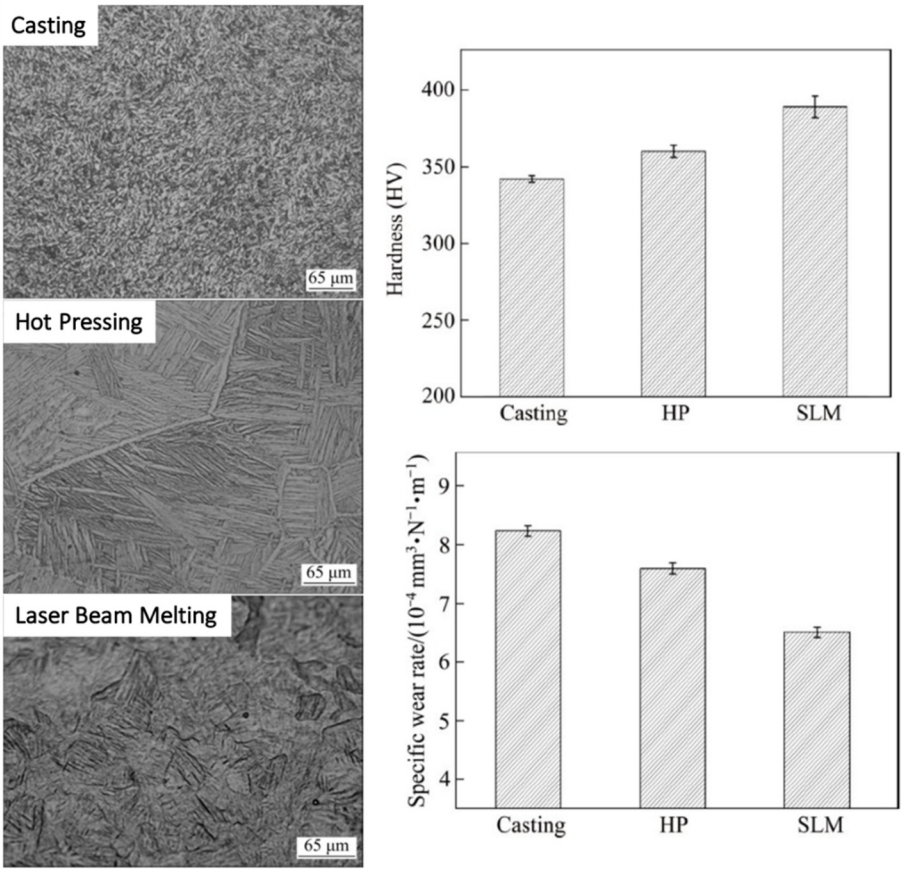

Figure 12. Optical micrographs, phase content (%), hardness and wear rate of Ti6Al4V fabricated by different processing routes (adapted with permission from [2]. Copyright 2017 Elsevier).

4. Conclusions

This review covered 132 studies relevant for a critical understanding of the mechanical properties of Ti6Al4V parts fabricated by Laser Powder Bed Fusion. This review was focused on the processing and microstructural parameters' influences on this alloy. Most of the published studies on Ti6Al4V manufactured by LPBF report near full density and superior strength to that obtained when using conventional processing routes (such as cast or wrought). When regarding tensile testing, the available results available show that typical Laser Powder Bed–Fused Ti6Al4V tensile properties (>900 MPa yield strength and >1000 MPa tensile strength) are adequate when considering the minimum values of the standards for implants and for aerospace applications (e.g., ASTM F136–13; ASTM F1108–14; AMS4930; AMS6932). It is important to highlight that heat treatments are an excellent method to obtain the best compromise between strength and ductility for a given application. For instance, for surgical implant applications, the best compromise between strength and ductility can be obtained by performing a heat treatment at 850° for 2 h, followed by furnace cooling. The fatigue properties of Ti6Al4V alloy produced by Laser Powder Bed Fusion are dictated by three main aspects. The first is the densification level of the produced parts, which is defined by the processing parameters used in the fabrication.

When defects such as pores and lack of fusion are present in high amounts, the fatigue performance tends to be poor, and cracks can initiate either in the bulk or at the surface due to these defects. The second aspect is the microstructural features, as by performing thermal and thermo-mechanical post-treatments, it is possible to substantially improve the fatigue performance, and HIP seems to be the most effective post-treatment to increase the fatigue performance of this alloy. The surface condition has a crucial impact on the fatigue performance of this alloy, and regarding LPBF, the natural surface condition was found to be extremely detrimental, and the machining of LPBF as-built parts seems to be an effective way to enhance the fatigue performance of Ti6Al4V parts manufactured by this technology. Typically, LPBF Ti6Al4V in the as-built condition exhibits higher tensile strength, lower ductility and higher hardness, while after performing post-treatments (thermal), lower tensile strength, higher ductility and lower hardness are generally attained.

Author Contributions: Conceptualization, F.B., M.G., F.S.S. and G.M.; methodology, F.B.; investigation, F.B. and G.M.; resources, F.S.S.; writing— F.B.; writing—review and editing, F.B. and G.M.; visualization, F.B., M.G. and F.S.S.; supervision, G.M.; project administration, F.S.S. and G.M.; funding acquisition, F.S.S. and G.M. All authors have read and agreed to the published version of the manuscript.

Funding: This work was supported by FCT national funds, under national support to an R&D units grant, through the reference projects UIDB/04436/2020 and UIDP/04436/2020 and also through the projects ADD2MECBIO (PTDC/EME-EME/1442/2020) and Additive_Manufacturing to Portuguese Industry_POCI-01-0247- FEDER-024533.

Conflicts of Interest: The authors declare no conflict of interest.

References

1. AM Market Forecast. Available online: https://www.metal-am.com/am-market-forecast-to-reach-51-billion-by-2030/ (accessed on 7 June 2022).
2. Bartolomeu, F.; Buciumeanu, M.; Pinto, E.; Alves, N.; Silva, F.S.; Carvalho, O.; Miranda, G. Ti6Al4V biomedical alloy wear behavior—A comparison between selective laser melting, hot pressing and conventional casting. *Trans. Nonferrous Met. Soc. China* **2016**, *27*, 829–838. [CrossRef]
3. Bartolomeu, F.; Faria, S.; Carvalho, O.; Pinto, E.; Alves, N.; Silva, F.; Miranda, G. Predictive models for physical and mechanical properties of Ti6Al4V produced by Selective Laser Melting. *Mater. Sci. Eng. A* **2016**, *663*, 181–192. [CrossRef]
4. Chastand, V.; Tezenas, A.; Cadoret, Y.; Quaegebeur, P.; Maia, W.; Charkaluk, E. Fatigue characterization of Titanium Ti-6Al-4V samples produced by Additive Manufacturing. *Procedia Struct. Integr.* **2016**, *2*, 3168–3176. [CrossRef]
5. Khorasani, M.; Ghasemi, A.; Rolfe, B.; Gibson, I. Additive manufacturing a powerful tool for the aerospace industry. *Rapid Prototyp. J.* **2022**, *28*, 87–100. [CrossRef]
6. Bordin, A.; Sartori, S.; Bruschi, S.; Ghiotti, A. Experimental investigation on the feasibility of dry and cryogenic machining as sustainable strategies when turning Ti6Al4V produced by Additive Manufacturing. *J. Clean. Prod.* **2016**, *142*, 4142–4151. [CrossRef]
7. Nicoletto, G. Anisotropic high cycle fatigue behavior of Ti–6Al–4V obtained by powder bed laser fusion. *Int. J. Fatigue* **2016**, *94*, 255–262. [CrossRef]
8. Linares, J.-M.; Chaves-Jacob, J.; Lopez, Q.; Sprauel, J.-M. Fatigue life optimization for 17-4Ph steel produced by selective laser melting. *Rapid Prototyp. J.* 2022; *ahead-of-print*. [CrossRef]
9. Montalbano, T.; Briggs, B.N.; Waterman, J.L.; Nimer, S.; Peitsch, C.; Sopcisak, J.; Trigg, D.; Storck, S. Uncovering the coupled impact of defect morphology and microstructure on the tensile behavior of Ti-6Al-4V fabricated via laser powder bed fusion. *J. Mater. Process. Technol.* **2021**, *294*, 117113. [CrossRef]
10. Costa, M.; Lima, R.; Melo-Fonseca, F.; Bartolomeu, F.; Alves, N.; Miranda, A.; Gasik, M.; Silva, F.; Silva, N. Development of β-TCP-Ti6Al4V structures: Driving cellular response by modulating physical and chemical properties. *Mater. Sci. Eng. C* **2019**, *98*, 705–716. [CrossRef]
11. Bartolomeu, F.; Abreu, C.; Moura, C.; Costa, M.; Alves, N.; Silva, F.; Miranda, G. Ti6Al4V-PEEK multi-material structures—Design, fabrication and tribological characterization focused on orthopedic implants. *Tribol. Int.* **2018**, *131*, 672–678. [CrossRef]
12. Bartolomeu, F.; Costa, M.; Alves, N.; Miranda, G.; Silva, F. Additive manufacturing of NiTi-Ti6Al4V multi-material cellular structures targeting orthopedic implants. *Opt. Lasers Eng.* **2020**, *134*, 106208. [CrossRef]
13. European Comission. *Additive Manufacturing in FP7 and Horizon 2020, Report from the EC Workshop on Additive Manufacturing Held on 18 June 2014*; 2014; 78p. Available online: https://www.rm-platform.com/linkdoc/ECAMWorkshopReport2014.pdf (accessed on 7 June 2022).

14. Bandyopadhyay, A.; Espana, F.; Balla, V.K.; Bose, S.; Ohgami, Y.; Davies, N.M. Influence of porosity on mechanical properties and in vivo response of Ti6Al4V implants. *Acta Biomater.* **2010**, *6*, 1640–1648. [CrossRef] [PubMed]
15. Taniguchi, N.; Fujibayashi, S.; Takemoto, M.; Sasaki, K.; Otsuki, B.; Nakamura, T.; Matsushita, T.; Kokubo, T.; Matsuda, S. Effect of pore size on bone ingrowth into porous titanium implants fabricated by additive manufacturing: An in vivo experiment. *Mater. Sci. Eng. C* **2016**, *59*, 690–701. [CrossRef] [PubMed]
16. Melo-Fonseca, F.; Lima, R.; Costa, M.; Bartolomeu, F.; Alves, N.; Miranda, A.; Gasik, M.; Silva, F.; Silva, N. 45S5 BAG-Ti6Al4V structures: The influence of the design on some of the physical and chemical interactions that drive cellular response. *Mater. Des.* **2018**, *160*, 95–105. [CrossRef]
17. Bartolomeu, F.; Costa, M.; Alves, N.; Miranda, G.; Silva, F. Engineering the elastic modulus of NiTi cellular structures fabricated by selective laser melting. *J. Mech. Behav. Biomed. Mater.* **2020**, *110*, 103891. [CrossRef] [PubMed]
18. Zhou, Y.; Abbara, E.M.; Jiang, D.; Azizi, A.; Poliks, M.D.; Ning, F. High-cycle fatigue properties of curved-surface AlSi10Mg parts fabricated by powder bed fusion additive manufacturing. *Rapid Prototyp. J.* 2022; *ahead-of-print*.. [CrossRef]
19. Giganto, S.; Martínez-Pellitero, S.; Cuesta, E.; Zapico, P.; Barreiro, J. Proposal of design rules for improving the accuracy of selective laser melting (SLM) manufacturing using benchmarks parts. *Rapid Prototyp. J.* 2022; *ahead-of-print*.. [CrossRef]
20. De Formanoir, C.; Michotte, S.; Rigo, O.; Germain, L.; Godet, S. Electron beam melted Ti–6Al–4V: Microstructure, texture and mechanical behavior of the as-built and heat-treated material. *Mater. Sci. Eng. A* **2016**, *652*, 105–119. [CrossRef]
21. Greitemeier, D.; Palm, F.; Syassen, F.; Melz, T. Fatigue performance of additive manufactured TiAl6V4 using electron and laser beam melting. *Int. J. Fatigue* **2016**, *94*, 211–217. [CrossRef]
22. *ISO 17296-2:2015*; Additive Manufacturing. General Principles. Part 2: Overview of Process Categories and Feedstock. ISO: Geneva, Switzerland, 2015.
23. Fan, Y.; Dong, D.; Li, C.; Sun, Y.; Zhang, Z.; Wu, F.; Yang, L.; Li, Q.; Guan, Y. Research and Experimental Verification on Topology-Optimization Design Method of Space Mirror Based on Additive-Manufacturing Technology. *Machines* **2021**, *9*, 354. [CrossRef]
24. Barbieri, L.; Muzzupappa, M. Performance-Driven Engineering Design Approaches Based on Generative Design and Topology Optimization Tools: A Comparative Study. *Appl. Sci.* **2022**, *12*, 2106. [CrossRef]
25. Holoch, J.; Lenhardt, S.; Revfi, S.; Albers, A. Design of Selective Laser Melting (SLM) Structures: Consideration of Different Material Properties in Multiple Surface Layers Resulting from the Manufacturing in a Topology Optimization. *Algorithms* **2022**, *15*, 99. [CrossRef]
26. Vaithilingam, J.; Goodridge, R.D.; Hague, R.J.; Christie, S.D.; Edmondson, S. The effect of laser remelting on the surface chemistry of Ti6al4V components fabricated by selective laser melting. *J. Mater. Process. Technol.* **2016**, *232*, 1–8. [CrossRef]
27. Sterling, A.J.; Torries, B.; Shamsaei, N.; Thompson, S.M.; Seely, D.W. Fatigue behavior and failure mechanisms of direct laser deposited Ti–6Al–4V. *Mater. Sci. Eng. A* **2016**, *655*, 100–112. [CrossRef]
28. Murr, L.; Quinones, S.; Gaytan, S.; Lopez, M.; Rodela, A.; Martinez, E.; Hernandez, D.; Medina, F.; Wicker, R. Microstructure and mechanical behavior of Ti–6Al–4V produced by rapid-layer manufacturing, for biomedical applications. *J. Mech. Behav. Biomed. Mater.* **2009**, *2*, 20–32. [CrossRef] [PubMed]
29. Tong, J.; Bowen, C.R.; Persson, J.; Plummer, A. Mechanical properties of titanium-based Ti–6Al–4V alloys manufactured by powder bed additive manufacture. *Mater. Sci. Technol.* **2016**, *33*, 138–148. [CrossRef]
30. Donachie, M.J., Jr. *Titanium: A Technical Guide*, 2nd ed.; ASM International: Novelty, OH, USA, 2000.
31. Kasperovich, G.; Haubrich, J.; Gussone, J.; Requena, G. Correlation between porosity and processing parameters in TiAl6V4 produced by selective laser melting. *Mater. Des.* **2016**, *105*, 160–170. [CrossRef]
32. Raju, R.; Duraiselvam, M.; Petley, V.; Verma, S.; Rajendran, R. Microstructural and mechanical characterization of Ti6Al4V refurbished parts obtained by laser metal deposition. *Mater. Sci. Eng. A* **2015**, *643*, 64–71. [CrossRef]
33. Shunmugavel, M.; Polishetty, A.; Littlefair, G. Microstructure and Mechanical Properties of Wrought and Additive Manufactured Ti-6Al-4V Cylindrical Bars. *Procedia Technol.* **2015**, *20*, 231–236. [CrossRef]
34. Hu, J.; Yang, S.; Shuai, Z.; Wang, X.; Xu, H. Microstructure Study on Large-Sized Ti–6Al–4V Bar Three-High Skew Rolling Based on Cellular Automaton Model. *Metals* **2022**, *12*, 773. [CrossRef]
35. Zhang, H.; Gao, T.; Chen, J.; Li, X.; Song, H.; Huang, G. Investigation on Strain Hardening and Failure in Notched Tension Specimens of Cold Rolled Ti6Al4V Titanium Alloy. *Materials* **2022**, *15*, 3429. [CrossRef] [PubMed]
36. Wang, X.; Zhou, G.; Men, Y.; Zhang, S.; Zhang, H.; Li, F.; Chen, L. Superplastic Deformation Behaviors and Power Dissipation Rate for Fine-Grained Ti-6Al-4V Titanium Alloy Processed by Direct Rolling. *Crystals* **2022**, *12*, 270. [CrossRef]
37. Geetha, M.; Singh, A.K.; Asokamani, R.; Gogia, A.K. Ti based biomaterials, the ultimate choice for orthopaedic implants—A review. *Prog. Mater. Sci.* **2009**, *54*, 397–425. [CrossRef]
38. Zhao, X.; Li, S.; Zhang, M.; Liu, Y.; Sercombe, T.B.; Wang, S.; Hao, Y.; Yang, R.; Murr, L.E. Comparison of the microstructures and mechanical properties of Ti–6Al–4V fabricated by selective laser melting and electron beam melting. *Mater. Des.* **2016**, *95*, 21–31. [CrossRef]
39. Bartolomeu, F.; Sampaio, M.; Carvalho, O.; Pinto, E.; Alves, N.; Gomes, J.; Silva, F.; Miranda, G. Tribological behavior of Ti6Al4V cellular structures produced by Selective Laser Melting. *J. Mech. Behav. Biomed. Mater.* **2017**, *69*, 128–134. [CrossRef] [PubMed]
40. Wang, X.; Xu, S.; Zhou, S.; Xu, W.; Leary, M.; Choong, P.; Qian, M.; Brandt, M.; Xie, Y.M. Topological design and additive manufacturing of porous metals for bone scaffolds and orthopaedic implants: A review. *Biomaterials* **2016**, *83*, 127–141. [CrossRef]

41. Edwards, P.; Ramulu, M. Fatigue performance evaluation of selective laser melted Ti–6Al–4V. *Mater. Sci. Eng. A* **2014**, *598*, 327–337. [CrossRef]
42. Liu, Q.; Wang, Y.; Zheng, H.; Tang, K.; Ding, L.; Li, H.; Gong, S. Microstructure and mechanical properties of LMD–SLM hybrid forming Ti6Al4V alloy. *Mater. Sci. Eng. A* **2016**, *660*, 24–33. [CrossRef]
43. Huang, H.; Lan, P.-H.; Zhang, Y.-Q.; Li, X.-K.; Zhang, X.; Yuan, C.-F.; Zheng, X.-B.; Guo, Z. Surface characterization and in vivo performance of plasma-sprayed hydroxyapatite-coated porous Ti6Al4V implants generated by electron beam melting. *Surf. Coat. Technol.* **2015**, *283*, 80–88. [CrossRef]
44. Furton, E.T.; Wilson-Heid, A.E.; Beese, A.M. Effect of stress triaxiality and penny-shaped pores on tensile properties of laser powder bed fusion Ti-6Al-4V. *Addit. Manuf.* **2021**, *48*, 102414. [CrossRef]
45. Capek, J.; Machova, M.; Fousova, M.; Kubásek, J.; Vojtěch, D.; Fojt, J.; Jablonská, E.; Lipov, J.; Ruml, T. Highly porous, low elastic modulus 316L stainless steel scaffold prepared by selective laser melting. *Mater. Sci. Eng. C* **2016**, *69*, 631–639. [CrossRef] [PubMed]
46. Kaufman, J.G.; Rooy, E.L. *Aluminum Alloy Castings: Properties, Processes And Applications*; ASM International: Materials Park, OH, USA, 2004.
47. Long, M.; Rack, H.J. Titanium alloys in total joint replacement—A materials science perspective. *Biomaterials* **1998**, *19*, 1621–1639. [CrossRef]
48. Miranda, G.; Araújo, A.; Bartolomeu, F.; Buciumeanu, M.; Carvalho, O.; Souza, J.; Silva, F.; Henriques, B. Design of Ti6Al4V-HA composites produced by hot pressing for biomedical applications. *Mater. Des.* **2016**, *108*, 488–493. [CrossRef]
49. Miranda, G.; Sousa, F.; Costa, M.; Bartolomeu, F.; Silva, F.; Carvalho, O. Surface design using laser technology for Ti6Al4V-hydroxyapatite implants. *Opt. Laser Technol.* **2019**, *109*, 488–495. [CrossRef]
50. Bartolomeu, F.; Costa, M.; Gomes, J.; Alves, N.; Abreu, C.; Silva, F.; Miranda, G. Implant surface design for improved implant stability—A study on Ti6Al4V dense and cellular structures produced by Selective Laser Melting. *Tribol. Int.* **2018**, *129*, 272–282. [CrossRef]
51. Bartolomeu, F.; Dourado, N.; Pereira, F.; Alves, N.; Miranda, G.; Silva, F. Additive manufactured porous biomaterials targeting orthopedic implants: A suitable combination of mechanical, physical and topological properties. *Mater. Sci. Eng. C* **2020**, *107*, 110342. [CrossRef]
52. Bartolomeu, F.; Fonseca, J.; Peixinho, N.; Alves, N.; Gasik, M.; Silva, F.; Miranda, G. Predicting the output dimensions, porosity and elastic modulus of additive manufactured biomaterial structures targeting orthopedic implants. *J. Mech. Behav. Biomed. Mater.* **2019**, *99*, 104–117. [CrossRef]
53. Song, B.; Zhao, X.; Li, S.; Han, C.; Wei, Q.; Wen, S.; Liu, J.; Shi, Y. Differences in microstructure and properties between selective laser melting and traditional manufacturing for fabrication of metal parts: A review. *Front. Mech. Eng.* **2015**, *10*, 111–125. [CrossRef]
54. Bartolomeu, F.; Buciumeanu, M.; Costa, M.; Alves, N.; Gasik, M.; Silva, F.; Miranda, G. Multi-material Ti6Al4V & PEEK cellular structures produced by Selective Laser Melting and Hot Pressing: A tribocorrosion study targeting orthopedic applications. *J. Mech. Behav. Biomed. Mater.* **2019**, *89*, 54–64. [CrossRef]
55. Kasperovich, G.; Hausmann, J. Improvement of fatigue resistance and ductility of TiAl6V4 processed by selective laser melting. *J. Mater. Process. Technol.* **2015**, *220*, 202–214. [CrossRef]
56. Leuders, S.; Thöne, M.; Riemer, A.; Niendorf, T.; Tröster, T.; Richard, H.; Maier, H. On the mechanical behaviour of titanium alloy TiAl6V4 manufactured by selective laser melting: Fatigue resistance and crack growth performance. *Int. J. Fatigue* **2013**, *48*, 300–307. [CrossRef]
57. Wolff, S.; Lee, T.; Faierson, E.; Ehmann, K.; Cao, J. Anisotropic properties of directed energy deposition (DED)-processed Ti–6Al–4V. *J. Manuf. Process.* **2016**, *24*, 397–405. [CrossRef]
58. Vilaro, T.; Colin, C.; Bartout, J.-D. As-Fabricated and Heat-Treated Microstructures of the Ti-6Al-4V Alloy Processed by Selective Laser Melting. *Met. Mater. Trans. A* **2011**, *42*, 3190–3199. [CrossRef]
59. Baufeld, B.; Van der Biest, O.; Gault, R. Additive manufacturing of Ti–6Al–4V components by shaped metal deposition: Microstructure and mechanical properties. *Mater. Des.* **2010**, *31*, S106–S111. [CrossRef]
60. SLM Solutions 125. Available online: https://www.slm-solutions.com/products-and-solutions/machines/slm-125/ (accessed on 6 June 2022).
61. SLM Solutions 280. Available online: https://slm280.slm-solutions.com/ (accessed on 6 June 2022).
62. EOS M280. Available online: https://cdn2.scrvt.com/eos/public/e1dc925774b24d9f/55e7f647441dc9e8fdaf944d18416bdb/systemdatasheet_M280_n.pdf (accessed on 6 June 2022).
63. EOS M290. Available online: https://cdn2.scrvt.com/eos/public/413c861f2843b377/93ef12304097fd70c866344575a4af31/EOS_System-DataSheet-EOS-M290.pdf (accessed on 6 June 2022).
64. Concept Laser GmbH M2 Cusing. Available online: https://www.concept-laser.de/fileadmin/user_upload/PDFs/1510_M2_cusing_EN.pdf (accessed on 6 June 2022).
65. Khorasani, A.M.; Gibson, I.; Ghaderi, A.; Mohammed, M.I. Investigation on the effect of heat treatment and process parameters on the tensile behaviour of SLM Ti-6Al-4V parts. *Int. J. Adv. Manuf. Technol.* **2019**, *101*, 3183–3197. [CrossRef]
66. Xu, W.; Brandt, M.; Sun, S.; Elambasseril, J.; Liu, Q.; Latham, K.; Xia, K.; Qian, M. Additive manufacturing of strong and ductile Ti–6Al–4V by selective laser melting via in situ martensite decomposition. *Acta Mater.* **2015**, *85*, 74–84. [CrossRef]

67. Xu, W.; Sun, S.; Elambasseril, J.; Liu, Q.; Brandt, M.; Qian, M. Ti-6Al-4V Additively Manufactured by Selective Laser Melting with Superior Mechanical Properties. *JOM* **2015**, *67*, 668–673. [CrossRef]
68. Popovich, A.A.; Sufiiarov, V.S.; Polozov, I.A.; Borisov, E.V. Microstructure and Mechanical Properties of Inconel 718 Produced by SLM and Subsequent Heat Treatment. *Key Eng. Mater.* **2015**, *651–653*, 665–670. [CrossRef]
69. Gong, H.; Rafi, K.; Gu, H.; Ram, G.D.J.; Starr, T.; Stucker, B. Influence of defects on mechanical properties of Ti–6Al–4V components produced by selective laser melting and electron beam melting. *Mater. Des.* **2015**, *86*, 545–554. [CrossRef]
70. Wycisk, E.; Emmelmann, C.; Siddique, S.; Walther, F. High Cycle Fatigue (HCF) Performance of Ti-6Al-4V Alloy Processed by Selective Laser Melting. *Adv. Mater. Res.* **2013**, *816–817*, 134–139. [CrossRef]
71. Rafi, H.K.; Starr, T.L.; Stucker, B.E. A comparison of the tensile, fatigue, and fracture behavior of Ti–6Al–4V and 15-5 PH stainless steel parts made by selective laser melting. *Int. J. Adv. Manuf. Technol.* **2013**, *69*, 1299–1309. [CrossRef]
72. Mower, T.M.; Long, M.J. Mechanical Behavior of Additive Manufactured and Powder Metallurgy Ti6Al4V. In Proceedings of the 13th World Conference on Titanium, San Diego, CA, USA, 16–20 August 2015; pp. 1331–1336.
73. Book, T.A.; Sangid, M.D. Strain localization in Ti-6Al-4V Widmanstätten microstructures produced by additive manufacturing. *Mater. Charact.* **2016**, *122*, 104–112. [CrossRef]
74. Greitemeier, D.; Donne, C.D.; Syassen, F.; Eufinger, J.; Melz, T. Effect of surface roughness on fatigue performance of additive manufactured Ti–6Al–4V. *Mater. Sci. Technol.* **2016**, *32*, 629–634. [CrossRef]
75. Liang, Z.; Sun, Z.; Zhang, W.; Wu, S.; Chang, H. The effect of heat treatment on microstructure evolution and tensile properties of selective laser melted Ti6Al4V alloy. *J. Alloys Compd.* **2018**, *782*, 1041–1048. [CrossRef]
76. He, B.; Wu, W.; Zhang, L.; Lu, L.; Yang, Q.; Long, Q.; Chang, K. Microstructural characteristic and mechanical property of Ti6Al4V alloy fabricated by selective laser melting. *Vacuum* **2018**, *150*, 79–83. [CrossRef]
77. Yan, X.; Yin, S.; Chen, C.; Huang, C.; Bolot, R.; Lupoi, R.; Kuang, M.; Ma, W.; Coddet, C.; Liao, H.; et al. Effect of heat treatment on the phase transformation and mechanical properties of Ti6Al4V fabricated by selective laser melting. *J. Alloys Compd.* **2018**, *764*, 1056–1071. [CrossRef]
78. Yan, X.; Yin, S.; Chen, C.; Jenkins, R.; Lupoi, R.; Bolot, R.; Ma, W.; Kuang, M.; Liao, H.; Lu, J.; et al. Fatigue strength improvement of selective laser melted Ti6Al4V using ultrasonic surface mechanical attrition. *Mater. Res. Lett.* **2019**, *7*, 327–333. [CrossRef]
79. Maskery, I.; Aremu, A.O.; Simonelli, M.; Tuck, C.; Wildman, R.; Ashcroft, I.; Hague, R. Mechanical Properties of Ti-6Al-4V Selectively Laser Melted Parts with Body-Centred-Cubic Lattices of Varying cell size. *Exp. Mech.* **2015**, *55*, 1261–1272. [CrossRef]
80. Huang, Q.; Liu, X.; Yang, X.; Zhang, R.; Shen, Z.; Feng, Q. Specific heat treatment of selective laser melted Ti–6Al–4V for biomedical applications. *Front. Mater. Sci.* **2015**, *9*, 373–381. [CrossRef]
81. Ali, H.; Ghadbeigi, H.; Mumtaz, K. Effect of scanning strategies on residual stress and mechanical properties of Selective Laser Melted Ti6Al4V. *Mater. Sci. Eng. A* **2018**, *712*, 175–187. [CrossRef]
82. Weißmann, V.; Bader, R.; Hansmann, H.; Laufer, N. Influence of the structural orientation on the mechanical properties of selective laser melted Ti6Al4V open-porous scaffolds. *Mater. Des.* **2016**, *95*, 188–197. [CrossRef]
83. Yan, C.; Hao, L.; Hussein, A.; Young, P. Ti–6Al–4V triply periodic minimal surface structures for bone implants fabricated via selective laser melting. *J. Mech. Behav. Biomed. Mater.* **2015**, *51*, 61–73. [CrossRef] [PubMed]
84. Günther, J.; Krewerth, D.; Lippmann, T.; Leuders, S.; Tröster, T.; Weidner, A.; Biermann, H.; Niendorf, T. Fatigue life of additively manufactured Ti–6Al–4V in the very high cycle fatigue regime. *Int. J. Fatigue* **2017**, *94*, 236–245. [CrossRef]
85. Riemer, A.; Richard, H.A. Crack Propagation in Additive Manufactured Materials and Structures. *Procedia Struct. Integr.* **2016**, *2*, 1229–1236. [CrossRef]
86. Leuders, S.; Vollmer, M.; Brenne, F.; Tröster, T.; Niendorf, T. Fatigue Strength Prediction for Titanium Alloy TiAl6V4 Manufactured by Selective Laser Melting. *Met. Mater. Trans. A* **2015**, *46*, 3816–3823. [CrossRef]
87. Dhansay, N.M.; Tait, R.; Becker, T. Fatigue and Fracture Toughness of Ti-6Al-4V Titanium Alloy Manufactured by Selective Laser Melting. *Adv. Mater. Res.* **2014**, *1019*, 248–253. [CrossRef]
88. Edwards, P.G.; Ramulu, M. Effect of build direction on the fracture toughness and fatigue crack growth in selective laser melted Ti-6Al-4V. *Fatigue Fract. Eng. Mater. Struct.* **2015**, *38*, 1228–1236. [CrossRef]
89. Palanivel, S.; Dutt, A.; Faierson, E.; Mishra, R. Spatially dependent properties in a laser additive manufactured Ti–6Al–4V component. *Mater. Sci. Eng. A* **2016**, *654*, 39–52. [CrossRef]
90. Promoppatum, P.; Onler, R.; Yao, S.-C. Numerical and experimental investigations of micro and macro characteristics of direct metal laser sintered Ti-6Al-4V products. *J. Mater. Process. Technol.* **2017**, *240*, 262–273. [CrossRef]
91. Emmelmann, C.; Scheinemann, P.; Munsch, M.; Seyda, V. Laser Additive Manufacturing of Modified Implant Surfaces with Osseointegrative Characteristics. *Phys. Procedia* **2011**, *12*, 375–384. [CrossRef]
92. Gong, H.; Rafi, K.; Gu, H.; Starr, T.; Stucker, B. Analysis of defect generation in Ti–6Al–4V parts made using powder bed fusion additive manufacturing processes. *Addit. Manuf.* **2014**, *1–4*, 87–98. [CrossRef]
93. Hassanin, H.; Modica, F.; El-Sayed, M.A.; Liu, J.; Essa, K. Manufacturing of Ti-6Al-4V Micro-Implantable Parts Using Hybrid Selective Laser Melting and Micro-Electrical Discharge Machining. *Adv. Eng. Mater.* **2016**, *18*, 1544–1549. [CrossRef]
94. Toptan, F.; Alves, A.C.; Carvalho, O.; Bartolomeu, F.; Pinto, A.; Silva, F.; Miranda, G. Corrosion and tribocorrosion behaviour of Ti6Al4V produced by selective laser melting and hot pressing in comparison with the commercial alloy. *J. Mater. Process. Technol.* **2018**, *266*, 239–245. [CrossRef]

95. Dai, N.; Zhang, L.; Zhang, J.; Chen, Q.; Wu, M. Corrosion behavior of selective laser melted Ti-6Al-4 V alloy in NaCl solution. *Corros. Sci.* **2016**, *102*, 484–489. [CrossRef]
96. Urlea, V.; Brailovski, V. Electropolishing and electropolishing-related allowances for powder bed selectively laser-melted Ti-6Al-4V alloy components. *J. Mater. Process. Technol.* **2017**, *242*, 1–11. [CrossRef]
97. Simonelli, M.; Tse, Y.Y.; Tuck, C. On the Texture Formation of Selective Laser Melted Ti-6Al-4V. *Met. Mater. Trans. A Phys. Metall. Mater. Sci.* **2014**, *45*, 2863–2872. [CrossRef]
98. Huang, Q.; Hu, N.; Yang, X.; Zhang, R.; Feng, Q. Microstructure and inclusion of Ti–6Al–4V fabricated by selective laser melting. *Front. Mater. Sci.* **2016**, *10*, 428–431. [CrossRef]
99. Antony, K.; Arivazhagan, N.; Senthilkumaran, K. Numerical and experimental investigations on laser melting of stainless steel 316L metal powders. *J. Manuf. Process.* **2014**, *16*, 345–355. [CrossRef]
100. Facchini, L.; Magalini, E.; Robotti, P.; Molinari, A.; Höges, S.; Wissenbach, K. Ductility of a Ti-6Al-4V alloy produced by selective laser melting of prealloyed powders. *Rapid Prototyp. J.* **2010**, *16*, 450–459. [CrossRef]
101. Cui, Y.; Cai, J.; Li, Z.; Jiao, Z.; Hu, L.; Hu, J. Effect of Porosity on Dynamic Response of Additive Manufacturing Ti-6Al-4V Alloys. *Micromachines* **2022**, *13*, 408. [CrossRef]
102. Baitimerov, R.M.; Lykov, P.A.; Radionova, L.V.; Safonov, E.V. Parameter optimization for selective laser melting of TiAl6V4 alloy by CO_2 laser. *IOP Conf. Ser. Mater. Sci. Eng.* **2017**, *248*, 012012. [CrossRef]
103. Khorasani, A.M.; Gibson, I.; Goldberg, M.; Littlefair, G. A survey on mechanisms and critical parameters on solidification of selective laser melting during fabrication of Ti-6Al-4V prosthetic acetabular cup. *Mater. Des.* **2016**, *103*, 348–355. [CrossRef]
104. Benedetti, M.; Torresani, E.; Leoni, M.; Fontanari, V.; Bandini, M.; Pederzolli, C.; Potrich, C. The effect of post-sintering treatments on the fatigue and biological behavior of Ti-6Al-4V ELI parts made by selective laser melting. *J. Mech. Behav. Biomed. Mater.* **2017**, *71*, 295–306. [CrossRef] [PubMed]
105. Vandenbroucke, B.; Kruth, J.-P. Selective laser melting of biocompatible metals for rapid manufacturing of medical parts. *Rapid Prototyp. J.* **2007**, *13*, 196–203. [CrossRef]
106. Vrancken, B.; Thijs, L.; Kruth, J.-P.; Van Humbeeck, J. Heat treatment of Ti6Al4V produced by Selective Laser Melting: Microstructure and mechanical properties. *J. Alloys Compd.* **2012**, *541*, 177–185. [CrossRef]
107. Koike, M.; Greer, P.; Owen, K.; Lilly, G.; Murr, L.E.; Gaytan, S.M.; Martinez, E.; Okabe, T. Evaluation of Titanium Alloys Fabricated Using Rapid Prototyping Technologies—Electron Beam Melting and Laser Beam Melting. *Materials* **2011**, *4*, 1776–1792. [CrossRef]
108. Wysocki, B.; Maj, P.; Sitek, R.; Buhagiar, J.; Kurzydłowski, K.J.; Świeszkowski, W. Laser and Electron Beam Additive Manufacturing Methods of Fabricating Titanium Bone Implants. *Appl. Sci.* **2017**, *7*, 657. [CrossRef]
109. Lu, S.; Qian, M.; Tang, H.; Yan, M.; Wang, J.; StJohn, D. Massive transformation in Ti–6Al–4V additively manufactured by selective electron beam melting. *Acta Mater.* **2015**, *104*, 303–311. [CrossRef]
110. Gu, D.; Hagedorn, Y.-C.; Meiners, W.; Meng, G.; Batista, R.J.S.; Wissenbach, K.; Poprawe, R. Densification behavior, microstructure evolution, and wear performance of selective laser melting processed commercially pure titanium. *Acta Mater.* **2012**, *60*, 3849–3860. [CrossRef]
111. Benedetti, M.; Cazzolli, M.; Fontanari, V.; Leoni, M. Fatigue limit of Ti6Al4V alloy produced by Selective Laser Sintering. *Procedia Struct. Integr.* **2016**, *2*, 3158–3167. [CrossRef]
112. Liu, S.; Shin, Y.C. Additive manufacturing of Ti6Al4V alloy: A review. *Mater. Des.* **2018**, *164*, 107552. [CrossRef]
113. Chen, Q.; Thouas, G.A. Metallic implant biomaterials. *Mater. Sci. Eng. R Rep.* **2015**, *87*, 1–57. [CrossRef]
114. Huang, C.; Yan, X.; Zhao, L.; Liu, M.; Ma, W.; Wang, W.; Soete, J.; Simar, A. Ductilization of selective laser melted Ti6Al4V alloy by friction stir processing. *Mater. Sci. Eng. A* **2019**, *755*, 85–96. [CrossRef]
115. Soro, N.; Attar, H.; Wu, X.; Dargusch, M.S. Investigation of the structure and mechanical properties of additively manufactured Ti-6Al-4V biomedical scaffolds designed with a Schwartz primitive unit-cell. *Mater. Sci. Eng. A* **2018**, *745*, 195–202. [CrossRef]
116. Galarraga, H.; Warren, R.; Lados, D.; Dehoff, R.R.; Kirka, M.M.; Nandwana, P. Effects of heat treatments on microstructure and properties of Ti-6Al-4V ELI alloy fabricated by electron beam melting (EBM). *Mater. Sci. Eng. A* **2017**, *685*, 417–428. [CrossRef]
117. Kumar, P.; Ramamurty, U. Microstructural optimization through heat treatment for enhancing the fracture toughness and fatigue crack growth resistance of selective laser melted Ti 6Al 4V alloy. *Acta Mater.* **2019**, *169*, 45–59. [CrossRef]
118. Dallago, M.; Fontanari, V.; Torresani, E.; Leoni, M.; Pederzolli, C.; Potrich, C.; Benedetti, M. Fatigue and biological properties of Ti-6Al-4V ELI cellular structures with variously arranged cubic cells made by selective laser melting. *J. Mech. Behav. Biomed. Mater.* **2018**, *78*, 381–394. [CrossRef]
119. Blasón, S.; Correia, J.; Apetre, N.; Arcari, A.; De Jesus, A.M.; Moreira, P.; Fernandez-Canteli, A. Proposal of a fatigue crack propagation model taking into account crack closure effects using a modified CCS crack growth model. *Procedia Struct. Integr.* **2016**, *1*, 110–117. [CrossRef]
120. Rafi, H.K.; Karthik, N.V.; Gong, H.; Starr, T.L.; Stucker, B.E. Microstructures and Mechanical Properties of Ti6Al4V Parts Fabricated by Selective Laser Melting and Electron Beam Melting. *J. Mater. Eng. Perform.* **2013**, *22*, 3872–3883. [CrossRef]
121. Zhai, Y.; Galarraga, H.; Lados, D. Microstructure Evolution, Tensile Properties, and Fatigue Damage Mechanisms in Ti-6Al-4V Alloys Fabricated by Two Additive Manufacturing Techniques. *Procedia Eng.* **2015**, *114*, 658–666. [CrossRef]
122. Van Hooreweder, B.; Apers, Y.; Lietaert, K.; Kruth, J.-P. Improving the fatigue performance of porous metallic biomaterials produced by Selective Laser Melting. *Acta Biomater.* **2017**, *47*, 193–202. [CrossRef] [PubMed]

123. Kruth, J.-P.; Mercelis, P.; Van Vaerenbergh, J.; Froyen, L.; Rombouts, M. Binding mechanisms in selective laser sintering and selective laser melting. *Rapid Prototyp. J.* **2005**, *11*, 26–36. [CrossRef]
124. Song, B.; Dong, S.; Zhang, B.; Liao, H.; Coddet, C. Effects of processing parameters on microstructure and mechanical property of selective laser melted Ti6Al4V. *Mater. Des.* **2012**, *35*, 120–125. [CrossRef]
125. Attar, H.; Calin, M.; Zhang, L.C.; Scudino, S.; Eckert, J. Manufacture by selective laser melting and mechanical behavior of commercially pure titanium. *Mater. Sci. Eng. A* **2014**, *593*, 170–177. [CrossRef]
126. Sun, J.; Yang, Y.; Wang, D. Mechanical properties of a Ti6Al4V porous structure produced by selective laser melting. *Mater. Des.* **2013**, *49*, 545–552. [CrossRef]
127. Amaya-Vazquez, M.; Sánchez-Amaya, J.; Boukha, Z.; Botana, F. Microstructure, microhardness and corrosion resistance of remelted TiG2 and Ti6Al4V by a high power diode laser. *Corros. Sci.* **2012**, *56*, 36–48. [CrossRef]
128. Kao, W.; Su, Y.; Horng, J.; Chang, C. Tribological, electrochemical and biocompatibility properties of Ti6Al4V alloy produced by selective laser melting method and then processed using gas nitriding, CN or Ti-C:H coating treatments. *Surf. Coat. Technol.* **2018**, *350*, 172–187. [CrossRef]
129. Kumar, S.; Kruth, J.-P. Wear Performance of SLS/SLM Materials. *Adv. Eng. Mater.* **2008**, *10*, 750–753. [CrossRef]